

AD-A079 853

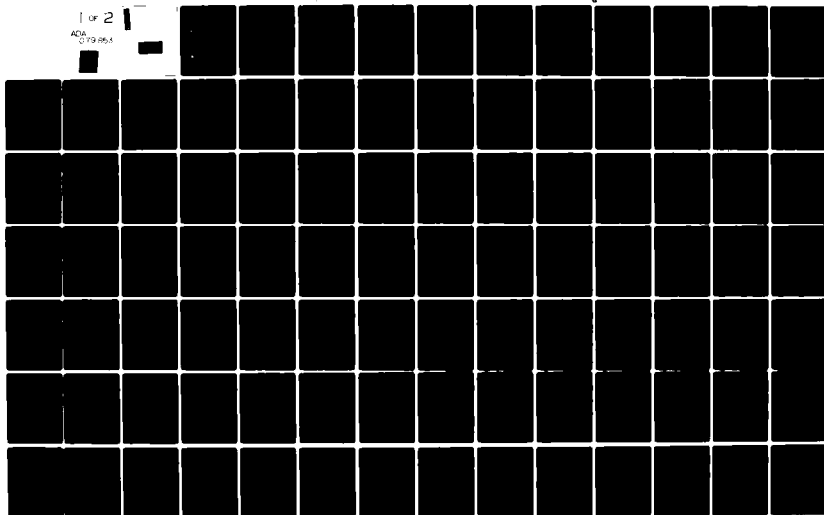
AIR FORCE INST OF TECH WRIGHT-PATTERSON AFB OH SCH00--ETC F/6 20/11
A STUDY OF SHORT CYLINDRICAL SHELLS WITH AND WITHOUT CUTOUTS UN--ETC(U)
DEC 79 C J BANG
AFIT/GA/AA/790-1

UNCLASSIFIED

NL

1 of 2

ADA
C19 853



14

AFIT/GA/AA/79D-1

ADA079853

9 Machine thesis

11 News 7-1

6

A STUDY OF SHORT CYLINDRICAL
SHELLS WITH AND WITHOUT
CUTOUTS UNDER PURE BENDING

THESIS 10

AFIT/GA/AA/79D-1

Carl J. Bang, Jr.
Captain USAF

12 1-17

DDC FILE COPY

Approved for public release; distribution unlimited

012 225

YK

A STUDY OF SHORT CYLINDRICAL SHELLS WITH AND
WITHOUT CUTOUTS UNDER PURE BENDING

THESIS

Presented to the Faculty of the School of Engineering
of the Air Force Institute of Technology
Air University
in Partial Fulfillment of the
Requirements for the Degree of
Master of Science

by

Carl J. Bang, Jr.
Captain USAF

Graduate Astronautical Engineering

December 1979

Approved for public release; distribution unlimited

Preface

I am sincerely grateful to Dr. Anthony Palazotto
for his patience and guiding efforts throughout this thesis.

I wish to thank my wife for her perseverance during this period while I was a part-time husband and father.

Accession for	
to	<input checked="checked" type="checkbox"/>
to	<input type="checkbox"/>
to	<input type="checkbox"/>
to	<input type="checkbox"/>
to	<input type="checkbox"/>
Distribution	
Available for	
Available for	
Special	

A

Contents

	Page
Preface	ii
List of Figures	iv
Symbols	vi
Abstract	ix
I. Introduction	1
Prologue	1
Background Theory and Literature Search	2
Stiffening and Cutouts	19
General Procedure	28
II. STAGS Procedures	30
STAGSC Theory	30
The Skogh-Brogan Routine	36
III. Modeling	42
Shell Model	42
Finite Difference Mesh Arrangements	48
IV. Results	51
Unstiffened Analyses	51
End Ring Stiffened Shells	62
Stringer Stiffened Shells With and Without Cutouts	64
V. Conclusions	80
Bibliography	83
Appendix A: Force and Moment Intensities, Constitutive Equations, Kinematic Relations	86
Appendix B: STAGSC Program Listings	89
Appendix C: Finite Difference Mesh Arrangements	96
Vita	104

List of Figures

Figure		Page
1.	Cylindrical Shell Segment	4
2a.	Bifurcation	7
2b.	Collapse	7
3.	Load Displacement Curves for Perfect and Imperfection Sensitive Structures	9
4.	Error Due to Neglect of Prebuckling Rota- tion Terms in Stability Equations for Uniform Lateral Pressure	11
5.	Ovalization of the Cross Section	15
6.	Load Deflection Curves	17
7.	Critical Load Factors for Cylinders Under Bending	18
8.	Primary Eccentricity Effect	22
9.	Secondary Eccentricity Effect	23
10.	Prebuckling and Buckling Displacements of an Internally Stiffened Simply Supported Cyl.	24
11.	Summary of Analytical Procedures	32
12.	STAGSA and STAGSC Finite Difference Schemes	34
13.	Applied Bending Moment Through Uniformly Varying Axial Loading	37
14.	Displaced Free End	39
15.	Pure Bending Rotation	42
16.	Shell, Stringer Geometry and Sign Conv.	43
17.	Boundary Conditions for the Shell Model	45
18.	Comparison of Axial Compressive Failure Loads Under Force (SS4) and Displacement (SS3) Conditions	46

Figure		Page
19.	Buckling Stress Intensities vs Mesh Size For Pure Bending and Axial Compression of an Unstiffened Cylinder	57
20.	Prebuckling Deflections For Unstiffened Cylinder	58
21.	Top View of an Unstiffened Cylinder Under Pure Bending	59
22.	Length to Radius Effects For an Unstiffened Cylinder With an Applied End Rotation	60
23.	W vs V Deflection for Given L/R Ratios of an Unstiffened Cylinder With an Applied End Rotation	61
24.	The Effect of Ring Stiffening on Pure Bending Induced Displacements	63
25.	Prebuckling Deflections for Stiffened Cylinder	71
26.	Prebuckling Deflections for Stringer Stiffened Cylinder with 1 Cutout	72
27.	Prebuckling Deflections for Stringer Stiffened Cylinder with 2 Cutouts	73
28.	Axial Compression vs Pure End Rotation Buckling Stress Intensities for Stiffened Cylinders With and Without Cutouts	74
29.	Buckling Moment vs Length For Stiffened Cylinders With and Without Cutouts Under Pure End Rotation.....	75
30.	Eigenvectors for Axial Compression and Pure Bending Loading of a Stiffened Cylinder	76
31.	Eigenvectors for Axial Compression and Pure Bending Loading of a Stiffened Cylinder With Two Symmetrical Cutouts	77
32.	Stress Intensity Flow For Axial Compression and Pure Bending Loading of a Stiffened Cylinder at Buckling	78
33.	Calculated Loading Ratio Above Cutout vs Change in Length For A Stiffened Cylinder ...	79

Symbols

a	half width of square cutout
A, A_1	stringer cross-sectional area
b_1	distance between stringers
b_{str}	width of rectangular stringer
C	$Et/(1-\nu^2)$ - extensional stiffness parameter
D	$Et^3/12(1-\nu^2)$ - bending stiffness parameter
e_1	distance between centroid of stringer and middle of shell surface
E	modulus of elasticity
F	vector of external forces
F_L	vector of external forces for linear solution
G	shear modulus
GJ	torsional stiffness of stringer
I_1	stringer moment of inertia
L	cylinder length
L'_x	derivative of stiffness operator
M	$\nabla R^2 N$ - applied bending moment or the resulting moment due to an applied end rotation
M_{cr}	total moment at buckling
M_{cl}	$.6 \nabla R t^2 E$ - classical buckling moment value
M_x, M_θ	moment resultants or intensities
\bar{M}_x	geometric bending stiffness of stringer-shell cross-section
m	number of circumferential waves

N	normal force
N_x, N_θ	normal and shearing force intensities or stress resultants
N_{cr}	buckling stress intensity
N_{cl}	classical buckling stress intensity
n	number of axial waves
P	applied end load
P_{cr}	buckling or critical load
P_{cl}	$2\pi R t \sigma_{cl}$ - classical buckling load of unstiffened cylinder
Q_x	transverse shearing force intensity
R	radius of the cylinder
t	shell thickness
u, v, w	displacement in the axial, circumferential, and radial - (normal) directions
U	total strain energy
V	total potential energy
W	work done by external forces
$x, y-\theta, z$	coordinates in axial, circumferential, and radial directions
Z	$(1 - \nu^2)^{1/2} (L^2/Rt)$ - Batdorf cylinder parameter
z_1	distance between shell mid-surface and combined stringer-shell centroid
β_x, β_θ	rotations in the designated direction
δ	displacement; variation
ϵ_x, γ_{xy}	strain components
κ_x, κ_{xy}	curvature change and twist

ν	Poisson's ratio
σ_x, τ_{xy}	stress components
σ_{cl}	$2\pi Et^3 / \{3(1-\nu^2)\}^{1/2}$ - classical buckling stress
ϕ	angle of applied end rotation

Abstract

In this report, short cylindrical shells are studied under pure bending. An edge kinematic constraint loading method is adapted for use with the STAGSC computer code. With it, short unstiffened cylindrical shells are studied for prebuckling displacements and compared with axially stressed cylinders. End rings are added to note their influence. The bending is applied to short internally stiffened (smeared stringer theory) cylinders, with the resulting buckling values and patterns contrasted against axial loading. The L/R range of interest is from .698 to 1.361. Symmetrical and unsymmetrical 12 inch cuts are added to the stiffened cylinder to study the resulting effects from this imperfection. The results indicate:

- a. For short length ($L/R < 10$) cylinders, end loading by pure bending causes structural deformation patterns different than long cylinder bending deflections.
- b. The imposed boundary effect for unstiffened cylinders diminishes with L/R increase until $L/R = 20$ where there is no noticeable deformation influence.
- c. End ring stiffeners studied did not alter the basic short cylinder deformation patterns.
- d. Compressive zone buckling failure under bending can be modeled through axial compression analysis.

A STUDY OF SHORT CYLINDRICAL SHELLS WITH AND WITHOUT CUTOUTS UNDER PURE BENDING

I. Introduction

Prologue

Anyone having bent a can or slender tube has witnessed cylindrical shell instability. More important manifestations include kinking of ocean floor piping, nuclear plant fluid pipe failures, and the failure of aircraft fuselages or spacecraft boosters. The aerospace design engineer is faced with trying to optimize the strength to weight characteristics of these flight structures. This compels him to understand the problems of thin shell stability and methods for determining design characteristics. It was this sort of impetus that motivated Donnell (Ref 16) to develop his simplified equations of equilibrium for a cylindrical wall in 1933. The high speed computer has greatly enhanced the ability to analyze and understand thin shell structures. I will use one such computer code (STAGSC) to analyze the effects of pure bending on short cylinders.

The thesis topic arose from discussions with Dr. Palazotto. A previous student, Norton Compton (Ref 15) had problems in keeping the end plane from warping when he

attempted to apply pure bending moments. My task became one of finding a method for applying pure end rotation while keeping the end plane undistorted and circular. Once the method was perfected, I was to study its effects on stiffened and unstiffened cylindrical shells with and without cutouts. Through an associate, Dr. Palazotto received a method devised by Jörgen Skogh and Frank Brogan (Ref 29), which I adapted for STAGSC (Ref 5). This paper will cover previous work in bending analyses, the Skogh routine, and results of employing it.

Background Theory and Literature Search

A shell structure is usually defined as a body enclosed between two closely spaced curved surfaces. Cylinders are a subset in that there is only one radius of curvature. Shell theory is an attempt to use the assumption of smallness in the thickness direction to relate the three-dimensional problem of deformation of the body to that of displacement components on a middle surface or reference surface. The analysis therefore involves making assumptions about the shells' dimensions. For thin cylindrical shells the following assumptions given by Love are standard (Ref 25):

1. The shell is thin. This means that the thickness of the shell is small compared with the radius of

curvature R of the middle surface, so that the ratio is small compared to unity.

2. The deflections of the shell are small, and the strains in the direction of the normal are small enough to be neglected. This allows us to refer the analysis to the initial configuration of the shell.

3. The normal stresses acting on planes parallel to the middle surface are negligible compared with other stress components and may be neglected in the stress-strain relations. This assumption will generally be valid except in the vicinity of highly concentrated loads.

4. The components of the displacements are linearly distributed across the thickness.

5. The shear strains which cause the distortions of the normals to the middle surface can be neglected. Which says that normals to the undeformed middle surface remain normal to it after deformation.

Assumptions 2, 3 and 5 are the shell counterparts for the Kirchhoff assumptions of thin plate theory (Ref 14). For a complete listing of the assumptions for Kirchhoff's theory of plates and Love's first approximation to the theory of shells, see Gould (Ref 17). These assumptions are applied to a portion of a shell surface, Fig 1, along with the internal forces and moments, expressed as forces and moments per unit distance (intensities) along the edge.

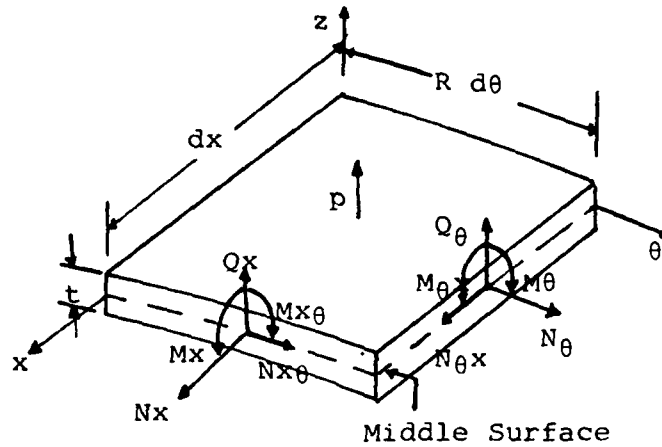


Figure 1. Cylindrical Shell Segment

On Fig 1, the N_x and N_θ are in plane normal intensities; $N_{x\theta}$ and $N_{\theta x}$ are shear intensities; Q_x and Q_θ are transverse shearing force intensities; the M_x and M_θ are bending moment intensities; and the $M_{x\theta}$ and $M_{\theta x}$ are twisting moment intensities. See Appendix A for their definitions along with the constitutive equations and kinematic relations. Allowing a slight deformed position, the forces are summed and recombined with the constitutive and middle surface kinematic relations to get equilibrium eqs with dead load pressure loading p :

$$RN_{x,x} + N_{x\theta,\theta} = 0$$

$$RN_{x\theta,x} + N_{\theta,\theta} = 0 \quad (1)$$

$$D\nabla^4 w + \frac{1}{R} N_\theta - (N_x w_{,xx} + \frac{2}{R} N_{x\theta} w_{,x\theta} + \frac{1}{R^2} N_{\theta\theta} w_{,\theta\theta}) = p$$

where $\nabla^4 w = w_{,xxxx} + \frac{2}{R^2} w_{,xx\theta\theta} + \frac{1}{R^4} w_{,\theta\theta\theta\theta}$

and D is the bending stiffness $D = \frac{Et^3}{12(1-\nu^2)}$

Equations (1) are coupled nonlinear partial differential equations for quasi-shallow cylindrical shells. Linear equations are obtained by deleting all quadratic and higher order terms in u , v , and w since they are products of already assumed small quantities. The resulting equations are:

$$\begin{aligned} RN_{x,x} + N_{x\theta,\theta} &= 0 \\ RN_{x\theta,x} + N_{\theta,\theta} &= 0 \\ D\nabla^4 w + \frac{1}{R} N_{\theta} &= p \end{aligned} \tag{2}$$

The difference between Eqs 2 and those for a flat plate is that Eq 2c is not uncoupled from Eq 2a and 2b. This gives us the important result that axial and/or circumferential movement produces radial displacements.

Eq 1 can be derived through the use of the minimum Potential Energy Criterion. A review of energy methods and variational calculus can be found in Brush (Ref 14) and Saada (Ref 25). The total potential energy V can be denoted as the sum of the strain energy U of the cylindrical shell and potential energy Ω of the applied forces. The condition for equilibrium is arrived at by taking the first variation of the total potential energy δV and setting

it equal to zero, while the criterion for stability is that, in addition, the second variation $\delta^2 V/2$ must be positive definite. For a cylindrical shell the strain energy U can be seen as a combination of a membrane strain energy U_m and bending strain energy U_b .

$$U_m = \frac{RC}{2} \iint \{ \epsilon_x^2 + \epsilon_\theta^2 + 2\nu \epsilon_x \epsilon_\theta + \frac{1-\nu}{2} \gamma_{x\theta}^2 \} dx d\theta \quad (3)$$

$$U_b = \frac{RD}{2} \iint \{ \kappa_x^2 + \kappa_\theta^2 + 2\nu \kappa_x \kappa_\theta + 2(1-\nu) \kappa_{x\theta}^2 \} dx d\theta \quad (4)$$

where C is the extensional stiffness $C = \frac{Et}{(1-\nu^2)}$.

And for the shell subjected to dead-load lateral pressure p , the potential energy is given by

$$\Omega = -R \iint p w dx d\theta \quad (5)$$

Setting the first variation δV equal to zero leads again to Eqs 1.

Before determining the buckling equations, a quick overview of stability theory is appropriate. Instability is a nonlinear phenomenon in which a small increase in load causes a disproportionately large increase in deformation. This load is called the critical load P_{cr} . The nonlinearity can be caused by either material (plasticity) or geometric nonlinearity. Only geometric nonlinearity is considered in this report. Sobel (Ref 30) details how the loss of stability can happen through either bifurcation buckling or geometric collapse. Figure 2a represents bifurcation

buckling. The load displacement curve emanating from the origin is intersected by another load displacement curve that represents a different equilibrium configuration. The point of intersection is called the bifurcation point, and the load at that point is called the bifurcation load. Figure 2b represents collapse. The load displacement is nonlinear from the origin and reaches a relative maximum. The load at this point is called the collapse load.

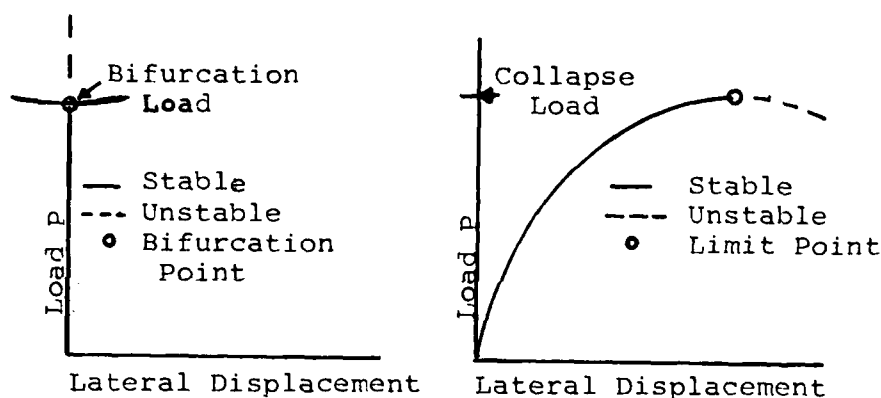


Figure 2a. Bifurcation

Figure 2b. Collapse

The adjacent-equilibrium path shown in Fig 2a is sloping upward indicating a stable post buckling path. This is not always so and in most cases does not happen. Koiter (Ref 18) studied the post buckling equilibrium configurations through the energy formulation of the loaded structure. The potential energy expression used earlier is of the general form

$$V = \int_A F(u,v,w,\lambda) dA \quad (6)$$

where u , v , and w are middle surface displacement components and λ is an applied load parameter.

Let the variables become

$$\begin{aligned} u &\rightarrow u_0 + u_1 \\ v &\rightarrow v_0 + v_1 \\ w &\rightarrow w_0 + w_1 \end{aligned} \tag{7}$$

where (u_0, v_0, w_0) represents an equilibrium position on the primary path, (u, v, w) form a nearby adjacent equilibrium position corresponding to the same value of λ , and (u_1, v_1, w_1) is a small infinitesimal displacement. Then when the change in potential energy is written

$$\Delta V = \frac{1}{2}\delta^2 V + \frac{1}{6}\delta^3 V + \frac{1}{24}\delta^4 V \dots \tag{8}$$

The first order term drops out since (u_0, v_0, w_0) is an equilibrium position. Application of the stationary potential energy criterion to the expression ΔV leads to the equations governing post buckling behavior. The cases shown in Fig 3 arise depending on the characteristics of the structure. As is seen in Fig 3 the post buckling paths vary considerably. The solid line secondary path represents perfect structure adjacent equilibrium, whereas the dash dot line denotes imperfection sensitivity. Notice that the imperfection sensitive lines are nonlinear from the origin and hence more closely model collapse modes. In all cases, the imperfections lower the load at which the structure becomes

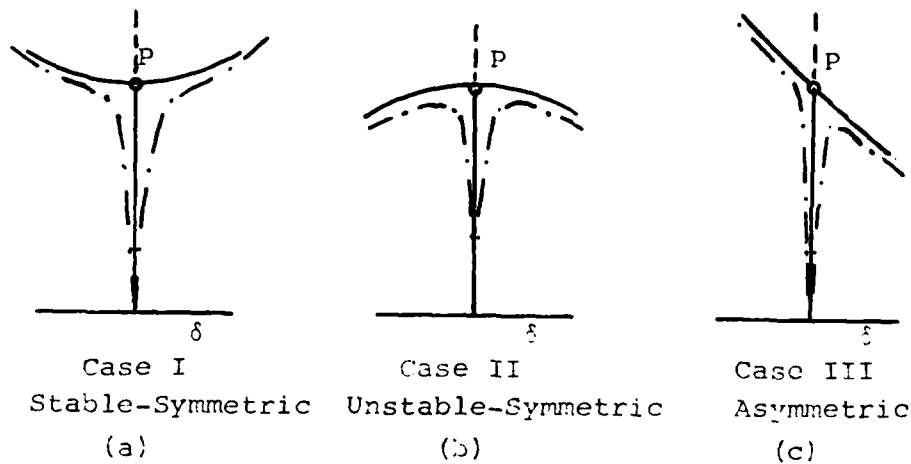


Figure 3. Load Displacement Curves For Perfect and Imperfection Sensitive Structures. From (30)

unstable. It is most critical in case II where the imperfect structure will snap at the limit point.

The equilibrium equations are now transformed into a linear coupled set representing the buckling mode. First, the reference surface displacement components are replaced by Eq 7, in Eq 1. Accordingly, the force intensities become

$$\begin{aligned}
 N_x &\rightarrow N_{x0} + \Delta N_x \\
 N_\theta &\rightarrow N_{\theta 0} + \Delta N_\theta \\
 N_{x\theta} &\rightarrow N_{x\theta 0} + \Delta N_{x\theta}
 \end{aligned}
 \tag{9}$$

Where terms with o subscripts refer to the primary equilibrium configuration, and ΔN_x , ΔN_θ , and $\Delta N_{x\theta}$ correspond to the change due to increment. When Eqs 7 and Eqs 9 are substituted into eqs 1, all terms in u_0 , v_0 , w_0 alone as

well as terms such as N_{x0} fall out. Also, if the higher order terms in u , v , w and N_x etc. are neglected due to their small relative size, the remaining equations become

$$\begin{aligned} RN_{x1,x} + N_{x01,\theta} &= 0 \\ RN_{x01,x} + N_{01,\theta} &= 0 \end{aligned} \quad (10)$$

$$\begin{aligned} D^4 w_1 + \frac{1}{R} N_{01} - \left[(N_{x0} w_{1,xx} + w_{0,xx} N_{x1}) \right. \\ \left. + \frac{2}{R} (N_{x0\theta} w_{1,x\theta} + w_{0,x\theta} N_{x01}) + \frac{1}{R^2} (N_{\theta0} w_{1,\theta\theta} + w_{0,\theta\theta} N_{01}) \right] = 0 \end{aligned}$$

The terms $w_{0,x}$ and $w_{0,\theta}$ represent prebuckling rotations which add considerable difficulty to the solution of these equations. Most early work (Refs 9; 15; 18) in this area neglected these terms in their analyses. With the computer available, these terms do not have to be neglected. However, a recent work by Brush (Ref 13) shows that at least for uniform lateral pressure the effect is very small. Figure 4 shows that for most thin cylinders the effect is less than 10%.

Therefore, neglecting the prebuckling rotations and substituting in the revised kinematic and constitutive relations we get a coupled set of three linear equations in the variables u_1 , v_1 , and w_1 . The solution to which is generally called the "buckling mode."

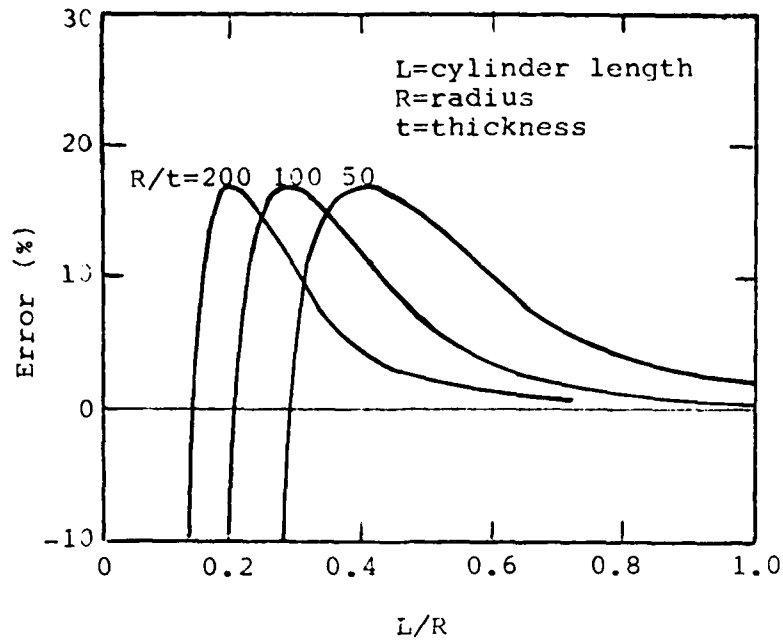


Figure 4. Error Due to Neglect of
Prebuckling-Rotation terms
in Stability Equations for
Uniform Lateral Pressure.
From (13)

$$R^2 u_{1,xx} + \frac{1-\nu}{2} u_{1,\theta\theta} + \frac{1+\nu}{2} R v_{1,x\theta} + \nu R w_{1,x} = 0$$

$$\frac{1+\nu}{2} R u_{1,x\theta} + \frac{1-\nu}{2} R^2 v_{1,xx} + v_{1,\theta\theta} + w_{1,\theta} = 0$$

$$D \nabla^4 w_1 + \frac{1}{R^2} C (v_{1,\theta} + w_1 + \nu R u_{1,x}) \quad (11)$$

$$- \left(N_{x\theta} w_{1,xx} + \frac{2}{R} N_{x\theta\theta} w_{1,x\theta} + \frac{1}{R^2} N_{\theta\theta\theta} w_{1,\theta\theta} \right) = 0$$

These are the Donnell stability equations in coupled form (Ref 16). They can be partially uncoupled to get the form which are homogeneous in w_1 . Using the partial derivative

notation $\frac{\partial}{\partial x}$ rather than the indicial notation and dropping the subscript, we get:

$$\begin{aligned}\nabla^4 u &= \frac{-\nu}{R} \frac{\partial^3 w}{\partial x^3} + \frac{1}{R^3} \frac{\partial^3 w}{\partial \theta^2 \partial x} \\ \nabla^4 v &= \frac{(2+\nu)}{R^2} \frac{\partial^3 w}{\partial \theta \partial x^2} + \frac{1}{R^4} \frac{\partial^3 w}{\partial \theta^3}\end{aligned}\quad (12)$$

$$D \nabla^4 w + \frac{1-\nu^2}{R^2} C \frac{\partial^4 w}{\partial x^4} - \nabla^4 \left(N_x \frac{\partial^2 w}{\partial x^2} + \frac{2}{R} N_{x\theta} \frac{\partial^2 w}{\partial \theta \partial x} + \frac{1}{R^2} N_\theta \frac{\partial^2 w}{\partial \theta^2} \right) = 0$$

It is Batdorf's (Ref 9) modification of these equations which Seide and Weingarten (Ref 26) used to study an isotropic cylinder under pure bending loads. Until the publication of (Ref 26) the prevailing method for figuring the buckling stress was by stating that $\sigma_b = 1.3\sigma_c$ where σ_b is the maximum bending stress and σ_c the critical axial stress for a corresponding axial compressive buckling problem. As Seide and Weingarten point out, the value 1.3 arose from Flugge's analysis where he expressed σ_b in terms of a dimensionless wavelength parameter $\lambda = m\pi R/L$; m denoting the number of axial half waves in the assumed sinusoidal buckle pattern. He found σ_b by minimizing σ_b with respect to λ . In doing so, he chose 1 for the value of λ to illustrate the technique, which led to $\sigma_b = 1.3\sigma_c$. Thus the value of 1.3 became part of engineering common practice. Seide and Weingarten used the Galerkin method to derive the stability criterion. They assumed the radial deflection

$$w = \sin \frac{m\pi x}{L} \sum_{n=0}^{\infty} a_n \cos n\theta \quad (13)$$

plugged it back into the modified Donnell equation and found the eigenvalue by matrix iteration of the determinant of coefficients for a_n . Their analysis showed that for all practical purposes $\sigma_b \approx \sigma_c$ for thin cylinders. Lakshmikantham (Ref 18) also used the Galerkin approach. He approximated the buckle pattern by

$$\begin{aligned} w &= A \sin (x/\lambda_x^*) \cos N\theta \text{ for } |\theta| \leq \pi/2N \\ &= 0 \text{ elsewhere on the circumference} \end{aligned} \quad (14)$$

which denotes a single lobe of variable width dependent on the value of N . He showed that, with the single dimple as the lowest energy state $\sigma_b \approx \sigma_c$ as above. This method also gave an upper bound $\sigma_b/\sigma_c = \pi/2$ when there exists many dimples along the top half of the cylinder. They were also able to establish that generally, the axial wavelength of pure bending is less than corresponding compressive case $\lambda_x^* \leq \lambda_x$ with the equality corresponding to the axisymmetric case. Thus the wavelength as well as the buckle pattern changes in going from the axial compression to bending problem. The wavelength is given by

$$\begin{aligned} \lambda_b \approx \lambda_c &= \frac{2\pi(Rt)^{1/2}}{[12(1-\nu^2)]^{1/2}} \text{ for } (R/t \text{ large}) \\ &= 3.45 (Rt)^{1/2} \text{ when } \nu = .3 \end{aligned} \quad (15)$$

It can be seen that this gives a wavelength quite small in comparison with the length of the shell.

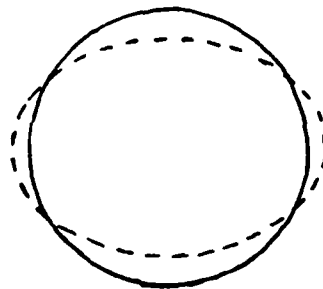
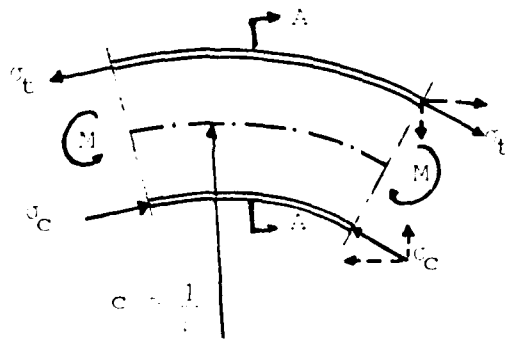
$$\frac{\lambda}{L} = 3.45 \left(\frac{R}{L}\right) \left(\frac{t}{R}\right)^{\frac{1}{2}} \ll 1 \quad (R/t \text{ large}) \quad (16)$$

More recent studies have also used the Galerkin approach. Reedy (Refs 22; 23) has used nondimensionalized parameters in the Batdorf modified Donnell equation. He uses $e^{-\beta\eta^2}$ for the circumferential modal form which allows him to match, for sufficiently small values of $\eta = R\theta/L$, an axial distribution of load which approximates $\cos \theta$.

The previous analyses have concentrated on thin, short to moderate length shells. As the cylindrical shell becomes longer, or for moderate length cylinders with ends that are not held circular, nonlinear prebuckling effects must be considered. Brazier (Ref 11) first studied this effect in 1927 (Ref Fig 5). He noticed that as an increasing moment is applied, the cross-section flattens and its moment of inertia decreases causing ovalization.

Due to the curvature, the axial stress in an arbitrary axial fiber will have a component (resultant) directed towards the neutral axis of bending. This happens on both the tension and compression sides. Sobel (Ref 31) lists the following consequences as a result of the oval shape.

1. A redistribution of stress occurs.
2. The circumferential radius of curvature increases.



Section A-A

Figure 5. Ovalization of the
Cross Section
From (7)

3. The bending stiffness of the cross-section is reduced as the moment increases.

4. Nonlinear collapse occurs at a moment lower than the one corresponding to bifurcation buckling from the linear membrane prebuckled state. Two types of nonlinear collapse modes are possible; the Brazier mode and the nonlinear wavy mode.

Brazier (Ref 11) determined the collapse mode by relating the strain energy to the applied moment through the curvature $M = \frac{\partial u}{\partial c}$ where $c = 1/\rho$. His results gave a maximum radial displacement,

$$w = \frac{2}{9} R \quad (17)$$

under an applied moment

$$M_{cr} = \frac{2\sqrt{2}}{9} \frac{EtRt^3}{\sqrt{1-\nu^2}} \quad (18)$$

and an axial stress

$$\sigma_{cr} = .33 Et/R \text{ for } \nu = .3 \quad (19)$$

which compares with

$$\sigma_{cr, \text{classical}} = .605 Et/R \quad (20)$$

for $\nu = .3$

Boundary conditions usually restrict the prebuckling deformations so that cross-sections at the shell edges remain circular. As a result, the flattening occurs at a higher stress than predicted by Brazier. However, as the L/R ratio increases, the influence of the flattening modes becomes dominant and the critical stresses approach that predicted by Brazier. Figure 6 (Refs 7; 31) details the relationship between the applied moment and the cross-sectional flattening.

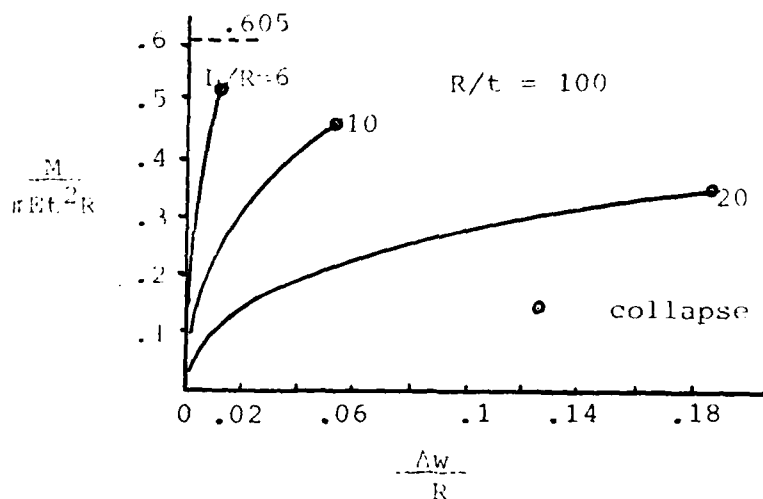


Figure 6. Load Deflection Curves From (7)

Akselr d (Ref 1) studied the Brazier effect to determine a relevant range over which the effect applies. An asymptotic method was used for the solution of the prebuckling problem while an equivalent cylinder approach was used to obtain the critical stress. He reported that σ_b varies from $.6Et/R$ for short cylinders to

$$\sigma_b = .295 Et/R \quad (R/t \text{ large}) \quad (21)$$

$$\approx 1/2 \sigma_{cr \text{ classical}}$$

for cylinders with

$$L/R \geq 2.5 (R/t)^{1/2} \quad (22)$$

His results are plotted against discrete points found by (Ref 7) in Fig 7.

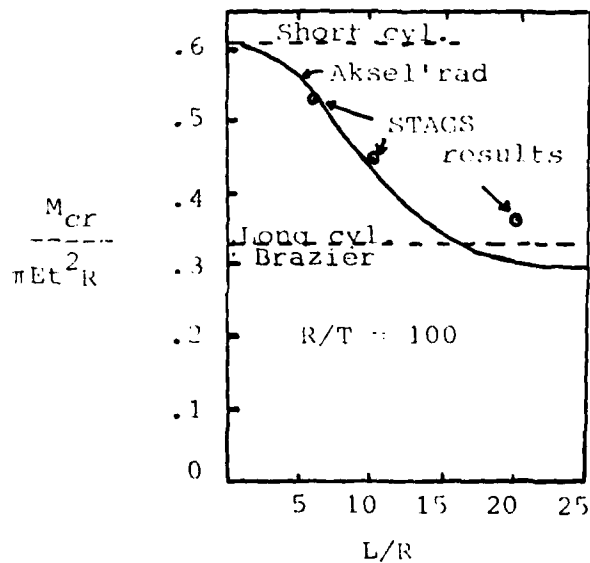


Figure 7. Critical Load Factors for Cylinders Under Bending from (7)

As was pointed out earlier, assuming the same boundary conditions are used, test results generally show a lower critical bending stress than theoretical, mostly due to imperfections within the testing specimens. And

since the cylinder under bending has less of its surface at the peak compression zone, when compared to axial compression, it is reasonable to expect that the maximum bending stress is higher than the critical axial stress. Sobel (Ref 31) outlines a method using a knock-down factor, which is an empirical reduction factor, that accounts for the discrepancy between classical predictions and experimental results. It is defined as

$$\gamma_{b,c} = \frac{\sigma_{cr \text{ experimental}}}{\sigma_{cr \text{ classical}}} \quad (23)$$

and applies to both bending and compression in the same fashion, respectively, but with different numerical values. If the ratio of bending to axial critical stress is taken, the following result is given

$$\frac{\sigma_b}{\sigma_c} = \frac{1-.731(1-e^{-\phi})}{1-.901(1-e^{-\phi})} \quad \text{where } \phi = \frac{1}{16} [R/t]^{\frac{1}{2}} \quad (24)$$

The picture, as to the buckling characteristics, changes greatly when internal and/or external stiffeners are added.

Stiffening and Cutouts

Stringers and rings are added to a structure to give rigidity and reduce imperfection sensitivity. If the stringers are closely spaced around the surface, the stiffened shell will fail through general instability. A

smeared stiffener theory can be used to analyze the total structure. Its assumptions (Refs 21; 27) are:

- a. The stiffeners are distributed over the whole surface of the shell.

- b. The normal strains vary linearly in the stiffener as well as in the shell. The normal strains in the stiffener and in the shell are equal at their point of contact.

- c. The shear membrane force N_{xy} is carried entirely by the shell.

- d. The torsional rigidity of the stiffener cross-section is added to the shell.

However, if the stiffeners are spaced relatively far apart the use of discrete theory is more appropriate. I will use the smeared theory option of STAGSC for my work. Singer et al. (Ref 28) did a parametric study via a Galerkin substitution in the Donnell stability equations. The results showed that stiffener eccentricity has a large effect on axially compressed cylinders. They classified the effects as

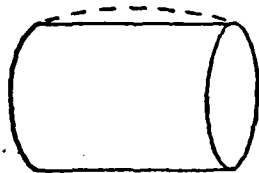
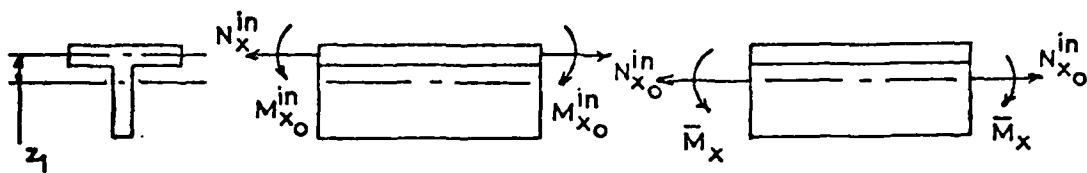
- a. Primary effect-*outside* stringers increase the actual bending stiffness in the longitudinal direction more than *inside* stringers.

- b. Secondary effect-*inside* stringers increase the actual extensional stiffness in the circumferential direction more than the *outside* stringers.

Figure 8 shows the primary effects whereas Figure 9 denotes the secondary effects. The eccentricity will either help or hinder a restoring moment when an initial displacement occurs in the radial direction. When the primary resistance to buckling is in the axial direction the restoring moment, M_x , remains constant regardless of the stiffener position. An additional moment is generated by the stiffeners with their resultant compressive force N_{x_0} acting through the distance z (the eccentricity--also given as e_1 on Fig 16). Thus, the actual moment produced by the shell-stiffener combination is different than the generated shell moment. As for the secondary effects, they come about due to an additional membrane force N_{y_0} produced in the hoop direction through Poisson's ratio acting on the additional axial strain caused by $M_{x_0}^{in}$. The radial component of this N_{y_0} will again assist or hinder buckling depending on stiffener location.

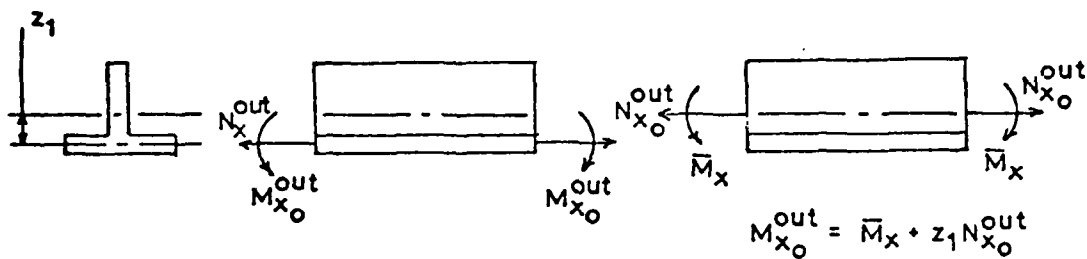
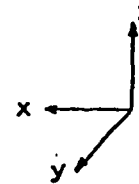
The preceding effects assume the radial displacements are either barrel shaped or continuously concave. Nelson (Ref 21) pointed out that stringer stiffened prebuckling axial wave patterns vary from concave to convex and hence should appear in the prebuckling analysis. STAGSC includes these effects in its linear prebuckling analysis.

Another aspect is where the load is applied in the shell-stiffener combination. Figure 10 from (Ref 6) depicts



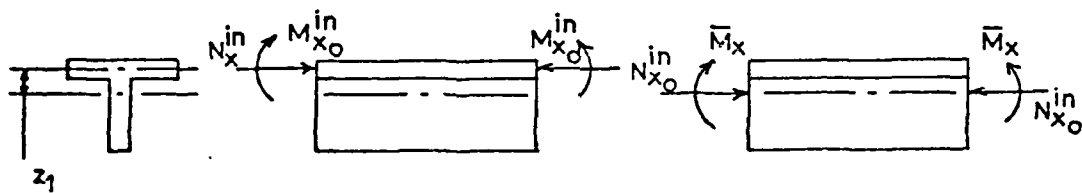
$$M_{x_0}^{in} = \bar{M}_x - z_1 N_{x_0}^{in}$$

POSITIVE WAVE - inside stringers

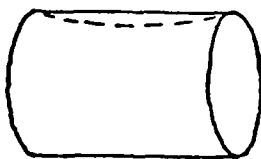


$$M_{x_0}^{out} = \bar{M}_x + z_1 N_{x_0}^{out}$$

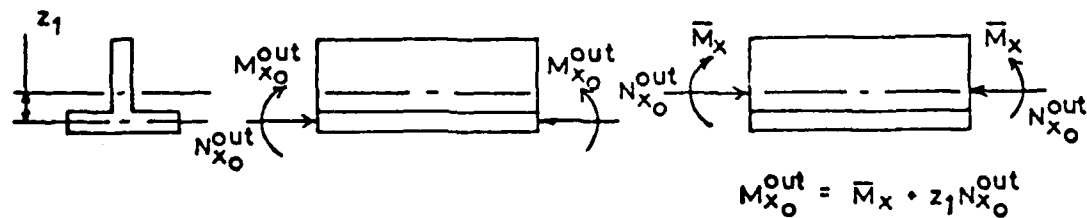
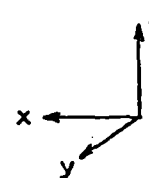
POSITIVE WAVE - outside stringers



$$M_{x_0}^{in} = \bar{M}_x - z_1 N_{x_0}^{in}$$



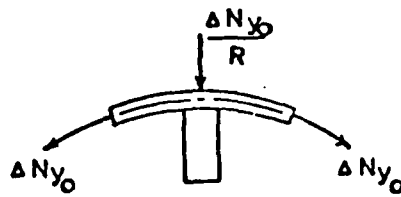
NEGATIVE WAVE - inside stringers



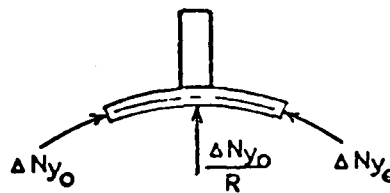
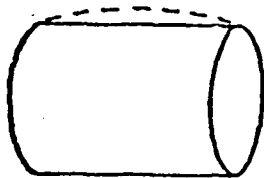
$$M_{x_0}^{out} = \bar{M}_x + z_1 N_{x_0}^{out}$$

NEGATIVE WAVE - outside stringers

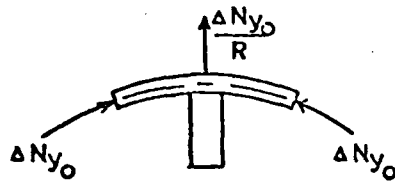
Figure 8. Primary Eccentricity Effect
From (28)



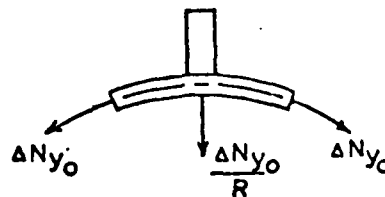
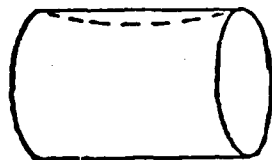
POSITIVE WAVE - inside stringers



POSITIVE WAVE - outside stringers



NEGATIVE WAVE - inside stringers



NEGATIVE WAVE - outside stringers

Figure 9. Secondary Eccentricity Effect
From (28)

the results of loading through the neutral surface versus loading at the centroid of the stiffeners.

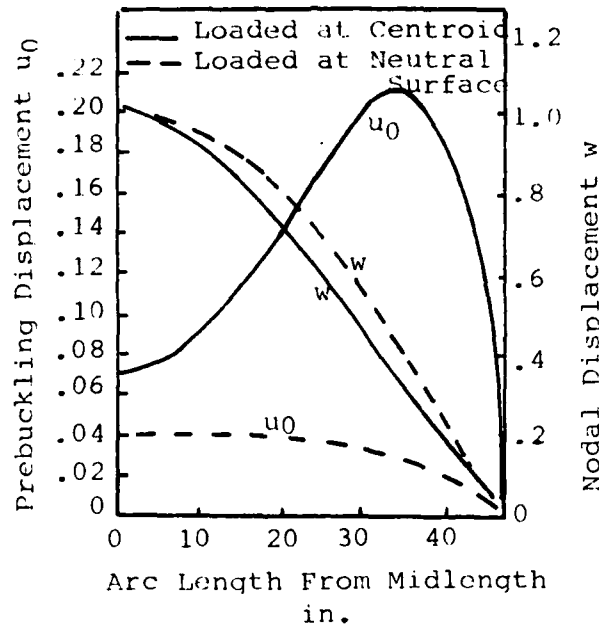


Figure 10. Prebuckling and Buckling Displacements of an Internally Stiffened Simply Supported Cyl. From (6)

It is apparent from the Fig 10 that the loading placement is very important for the prebuckling displacements but doesn't have too much of an effect on the buckling mode. Boundary conditions have more of an impact there.

Lakshmikantham et al. (Ref 19) studied the bending of orthotropic shells via the Galerkin procedure, using the same assumed deflection function as for the isotropic cylinder. They found $\sigma_b \approx \sigma_c$ as before where

$$\begin{aligned}\sigma_c &= 1 + 12(1-\nu^2)Z^2/\pi^4 & 0 \leq Z \leq Z^* \\ &= .702 Z(1-\nu^2)^{1/2} & Z^* \leq Z\end{aligned}\quad (25)$$

$$\text{where } Z^* = \pi^2 / [12(1-\nu^2)]^{1/2} \quad (26)$$

$$\text{and } Z = \frac{L^2}{Rt}(1-\nu^2)^{1/2} \text{ is the Batdorf parameter.} \quad (27)$$

Referring to (Refs 27; 28) further comments are possible. Singer noticed that for very small values of Z , that is less than 15, inside stiffened shells have analytical buckling loads greater than outside stiffened shells. Also, a decrease in eccentricity effect occurs for long shells, Z greater than 1000, where the cylinders act unstiffened. Also, contrasted against Z in the study were the stiffener parameters. It was noted that as the stiffener parameters increased, there was a corresponding increase in the eccentric stiffening except for very long shells. The results showed that the eccentricity affect behavior depends very heavily on the geometry of the shell; whereas, the stiffener geometry influences the magnitude of the eccentricity effect.

Along with the stiffener versus Z studies, the smeared stiffener theory was better defined. It was found that the nondimensional area ratio A_1/b_1t from Fig 16 is the important geometric parameter which determines whether smeared theory is suitable. Singer (Ref 27) concluded that

with a stiffener area ratio greater than 0.2 stringer stiffened shells could be analyzed closely with smeared theory.

Much study has also been directed towards the effects of different boundary conditions. Nelson's (Ref 21) thesis was devoted to a parameter study using the standard delineation of boundary constraints:

SS1	$W=0$	$W_{,xx}=0$	$N_x=0$	$N_{xy}=0$
SS2	$W=0$	$W_{,xx}=0$	$u=0$	$N_{xy}=0$
SS3	$W=0$	$W_{,xx}=0$	$N_x=0$	$v=0$
SS4	$W=0$	$W_{,xx}=0$	$u=0$	$v=0$

(26)

CC1	$W=0$	$W_{,x}=0$	$N_x=0$	$N_{xy}=0$
CC2	$W=0$	$W_{,x}=0$	$u=0$	$N_{xy}=0$
CC3	$W=0$	$W_{,x}=0$	$N_x=0$	$v=0$
CC4	$W=0$	$W_{,x}=0$	$u=0$	$v=0$

Some of his results were

a. For all the simply supported and clamped cylinders with and without cutouts, the $u=0$ axial restraint is the most important factor in buckling of axially compressed cylinders. For small values of L/R , the $v=0$ condition gains importance in simply supported stiffened cylinders.

b. For simply supported cylinders, with and without cutouts, internally stiffened cylinders are more sensitive to inplane boundary conditions.

c. The boundary conditions actually realized in experimental tests can be determined by correlating the experimental loads to the theoretical values for various boundary conditions. An agreement between results would then indicate the boundary conditions actually experienced in experimental tests.

Noting the latter conclusion, the differences between experimental tests and analytical studies arise from three areas: initial imperfections, prebuckling rotation, and boundary conditions. With judicious forethought the last two can be modeled closely whereas the first requires empirical studies.

Theoretical and experimental studies of cutout effects under bending are very sparse, if any. What studies have been accomplished have dealt mainly with cutout effects for axially compressed cylinders. Brogan and Almroth (Ref 12) studied an unstiffened shell with two symmetrical cutouts. Their theory indicated a collapse load, 30% above the experimental load of the shell with reinforced cutouts, was only slightly below the critical load for a cylinder without cutouts. When they compared their results against Tennyson's cylinders with circular holes, it was noticed that the rectangular holes have less of an effect. However, Brush and Almroth (Ref 14) have lately shown that the effect is approximately the same. Palazotto (Ref 22) carried out a much more thorough investigation of cutouts using the

STAGSA computer program. He showed that discrete and smeared theories give close results for a nodal arrangement which includes a circumferential mesh line at and between stringers and axial mesh spacing equal to the stringer spacing. This arrangement produced results within 3% of those with a more detailed mesh arrangement. Further, a mesh arrangement that insures at least five nodes per half sine wave was shown to be sufficient. Nelson (Ref 21) further studied the effects of smeared stringer reinforcement of the cutouts. He found that cutouts affected the externally stiffened shells to a greater extent than internally stiffened shells and this effect diminished as the L/R ratio increased. Also, he found that the influence of cutouts on the critical loads of stringer stiffened cylinders is analogous to the effects that initial geometric imperfections have on theoretical loads for "perfect" cylinders.

This introduction, although not complete as to all the studies which have been completed in this area, should serve as an overview of the subject.

General Procedure

The Skogh-Brogan bending moment routine (Ref 29) is combined with the STAGSC (Ref 5) computer code to analyze the effects on cylindrical cylinders. The L/R ratio is kept very short to minimize the Brazier effect. Using the linear bifurcation branch, a rotation is applied to cylinders

without stiffening. The impetus is to study the deflection buckling data. The cylinder L/R is then increased up to 20 to 1 to see how the bending boundary deflections are changed. Then, end rings are added to the shell to see how the near bending boundary deflections are effected. The last half of the study has stringers added to the cylinder for analysis, with and without 12" cutouts. The STAGSC smeared stiffener theory is used for this analysis. A parameter study is accomplished with the L/R ratio changing from .698 to 1.361.

II. STAGS Procedures

STAGSC Theory

References 2, 3, 4, 5, 6, and 13 contain to varying degrees the basis on which the STAGSC code is built. I recommend (Refs 3; 4) as a primer before employing the users manual (Ref 5), since the proposed theory section for the STAGSC manual was never published. Also, a newer version STAGSC-1 is now out in the field which mainly uses a finite element approach. Therefore, it will probably be harder in the future to get help with the STAGSC version. One advantage that the C-1 version should have, although it is not available yet, is a post-processing graphics package. For any structural code a picture representation is very much needed to get a grasp on what the surface is doing. Without it, the time devoted to plotting points makes that particular code less worthwhile. I will outline the basics of the STAGSC finite difference process in finding the buckling values, then indicate the major differences between STAGS A and C versions for finite difference analysis, and mention some of the facets involved in its smeared theory.

Structural behavior is governed by the equation

$$M\ddot{u} + D(\dot{u}) + B(u) + K(u) = F \quad (27)$$

where \underline{u} is a vector of displacement components, M is the mass matrix, D and B include forces that are functions of deformation velocity and structural deformation respectively, K is the generally nonlinear stiffness operator, and \underline{F} a vector of external forces. If the loads vary slowly all time derivatives can be neglected. Figure 11 comes from (Ref 4). It delineates the solution avenues available for the different applicable terms of Eq 27. Assuming the external forces vary very slowly and the load is independent of deformation, then STAGSC uses a potential energy method like Eq 6 to develop the applicable equations. A surface mesh is introduced and derivatives of the displacement components are expressed, using a truncated Taylor series expansion, in terms of the displacements at the mesh points by different approximations. Brush (Ref 14) gives a good introduction to the subject and solves an example column buckling problem. The derivative approximations are substituted into the strain energy equations. For stability, it was related earlier that the second variation of V is set equal to zero. Vanishing of the first variation of V leads to the equation

$$LX = F \quad (28)$$

where L is the stiffness operator that relates the finite nodal displacement vector X to the external forces. For the bifurcation problem if another displacement vector Y in the neighborhood of X satisfies the equation, then

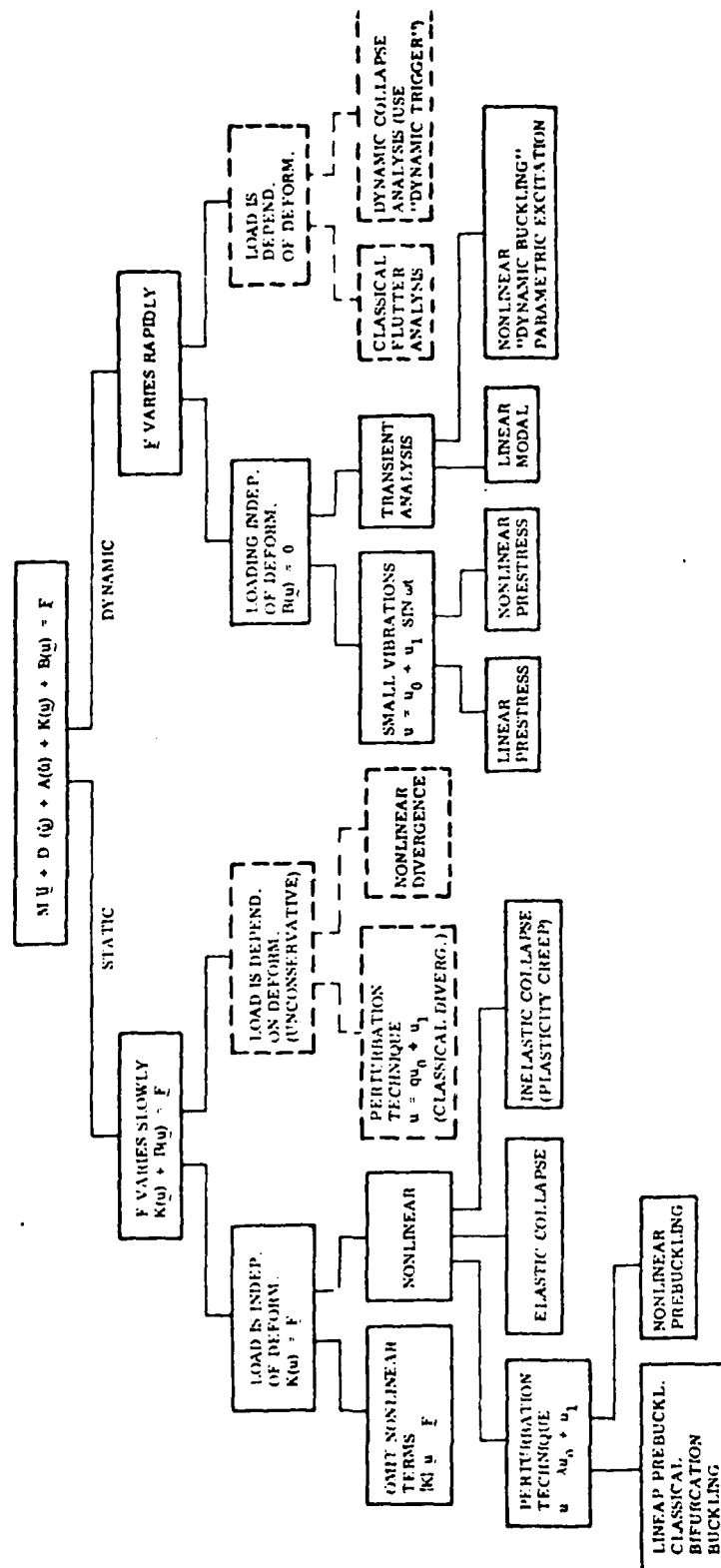


Figure 11. Summary of Analytical Procedures From (4)

$$LY = F \quad (29)$$

And since there can be multiple solutions to Eq 28, a necessary condition for bifurcation is that $L'x$ be a singular matrix where L' denotes the derivative of the stiffness operator. This leads to

$$\det (L'x) = 0 \quad (30)$$

It is then assumed that X may be written as

$$X = \lambda X_L \quad (31)$$

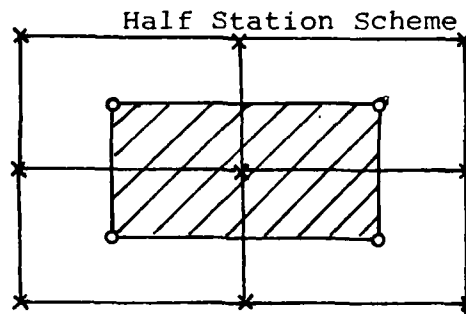
where X_L is a linear solution for the vector F_L ; this leads to Eq 30 becoming

$$\det (L'\lambda x_L) = 0 \quad (32)$$

This is equivalent to an algebraic eigenvalue problem. Its solution for λ gives the critical load as a multiple of the linear force vector F_L

$$F_{CR} = \lambda F_L \quad (33)$$

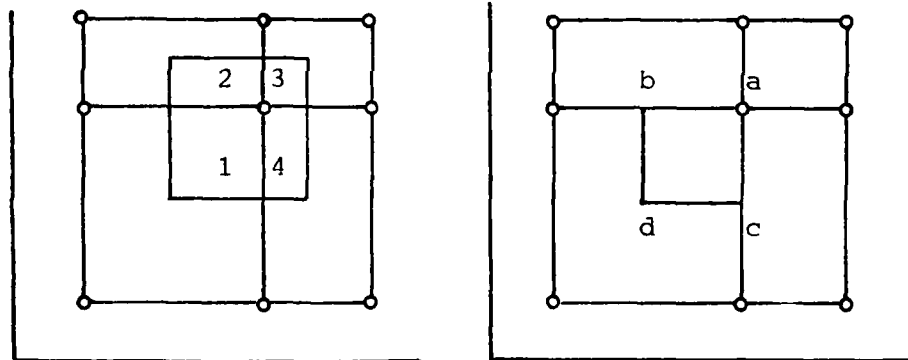
In this discussion, it was mentioned that a certain difference scheme is used to evaluate the derivatives. STAGSA was based on a half station scheme. See Fig 12 from (Ref 3). This scheme has a weakness in its inefficiency for nonlinear or stability analysis. It also has the disadvantage that in-plane displacements must be defined at fictitious points outside the shell boundaries. The STAGSC



w Defined
u,v Defined

STAGSA

STAGSC



Quantity Location

ϵ_x b

ϵ_y c

γ_{xy} d

Quantity Location

β_x b

β_y c

w_{xx} a

w_{yy} a

w_{xy} d

Figure 12. STAGSA and STAGSC Finite Difference Schemes
From (3)

version uses the whole station scheme. The point in question is surrounded by the total integration area broken down into 4 smaller regions. The corner of each smaller area has defined the requisite quantities, including the rotations. This method allows better convergence. It has been postulated in (Ref 3) that the finite difference approach converges toward the correct solution if:

1. The local truncation error vanishes with the gridsize.
2. For small values of nodal separation distance, the solution varies continuously with the input data loads.

It was brought out in the background section that Singer (Ref 27) gave several conditions for using the smeared stiffener analysis. Since, for my work the stiffener area ratio is $.9333 > .2$ recommended by Singer, the smeared theory is applicable. Brush (Ref 14), Lakshmikantham (Ref 19), and Singer (Ref 28) outline how smeared theory is incorporated into the equilibrium equation. It is handled through the generalized constitutive equations where the coupling effects are added to or subtracted from the existing stiffness parameters. As an example, the primary axial compression effect of a smeared stiffener is added to the membrane extensional stiffness parameter C expression. It has the form

$$C_{\text{new}} = C_{\text{old}} + \frac{EA_s}{ds} \quad (34)$$

where A_s , ds are the area of and distance between stringers.

The STAGSC (Ref 5) code lets the user detail the shell wall properties and dimensions, either directly through regular data cards or by a user written subroutine Wall. The program further handles the addition of smeared or discrete stiffeners along the surface, and the mesh grid size can be varied through specification in the discretization section. Since my analysis includes nonsymmetric cutouts, the regular data cards were unable to handle the specifications, and I had to use the user defined subroutine Wall to input my data. Appendix B contains two listings of the subroutine Wall. The first listing does not include cutout data whereas the second listing does. Although for the case of no cutouts (listing 1) the use of the Wall subroutine was not needed, I decided to use it for uniformity so that the cutout results could be compared directly. In both cases smeared theory was incorporated within the Wall subroutine. The mesh dimensions, surface parameters, stiffener configuration, and cutout relationships will be outlined in the modeling section of this report.

The Skogh-Brogan Routine

To apply pure bending moments, in previous work done with STAGS (Refs 5; 15; 32), an end line load N_x was varied around the edge uniformly with the cosine. (See Fig 13.)

$$N_x = -N \cos \theta \quad (35)$$

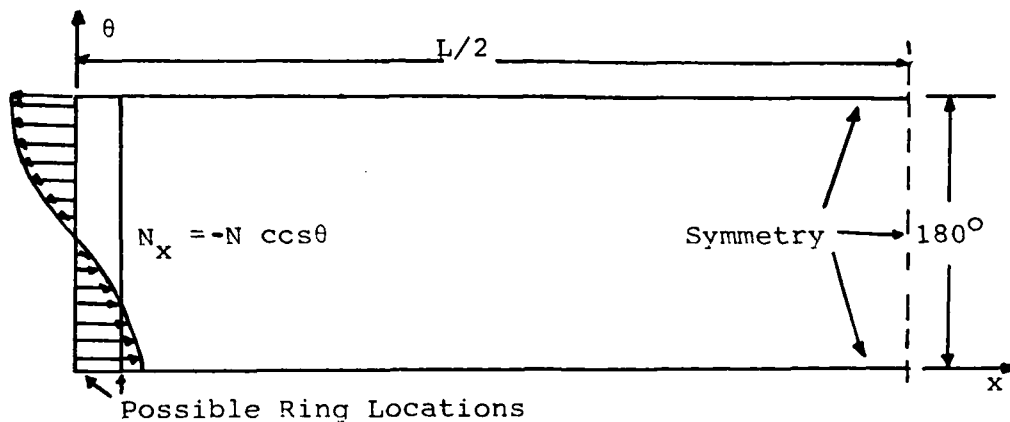


Figure 13. Applied Bending Moment Through Uniformly Varying Axial Loading

where N is the amplitude of the load and θ is the circumferential coordinate. The generated bending moment is therefore

$$M = N\pi R^2 \quad (36)$$

This method did impart the desired moment numerical values; however, it would also lead to some warping of the end plane resulting in a load that was not pure planer bending, and in some cases a net axial force also developed. End rings were used to try and counteract the warping tendency.

Mr. Jörgen Skogh and Frank Brogan (Ref 29) working at Lockheed's Palo Alto Research Laboratory approached the problem from a different viewpoint. They set out to enforce a planer end rotation and accept the applied moment value which resulted. They were able to accomplish this through the use of constraint equations which required that any

point on the end plane meet certain boundary kinematic restraint relationships. Thus free end rotation became the independent variable (see Fig 14). The free end of the cylinder is shown displaced through an angle ϕ which is assumed to be small so that $\cos \phi \approx 1$. The equations which they used to keep the end plane circular are

$$v \sin \theta - w \cos \theta = 0 \quad (37)$$

$$-v_0 + v \cos \theta + w \sin \theta = 0 \quad (38)$$

Eqs 37 and 38 keep the triangle formed by v , w , and v_0 (Fig 14) in equilibrium. That is why the angle ϕ should be kept small--to keep the length v_0 linear in Eq 38. The requirement that this circular end remain planar under rotation is fulfilled by

$$u_0 = (u_{90} - u_0) \sin \theta - u = 0 \quad (39)$$

This says that for any angle θ (position around the circle) the vertical distance u is a function of the difference $u_{90} - u_0$ as defined in Fig 14. By changing that difference, the distance u varies, changes for a given u_0 and θ . In effect, $u_{90} - u_0$ is a measure of the slope which has changed, meaning the angle of rotation has changed.

Skogh and Brogan's next ingenious step was to input this difference as a displacement on a "dummy" branch. The term dummy is used in the respect that this second branch is only used as a method for inputting data and has no other

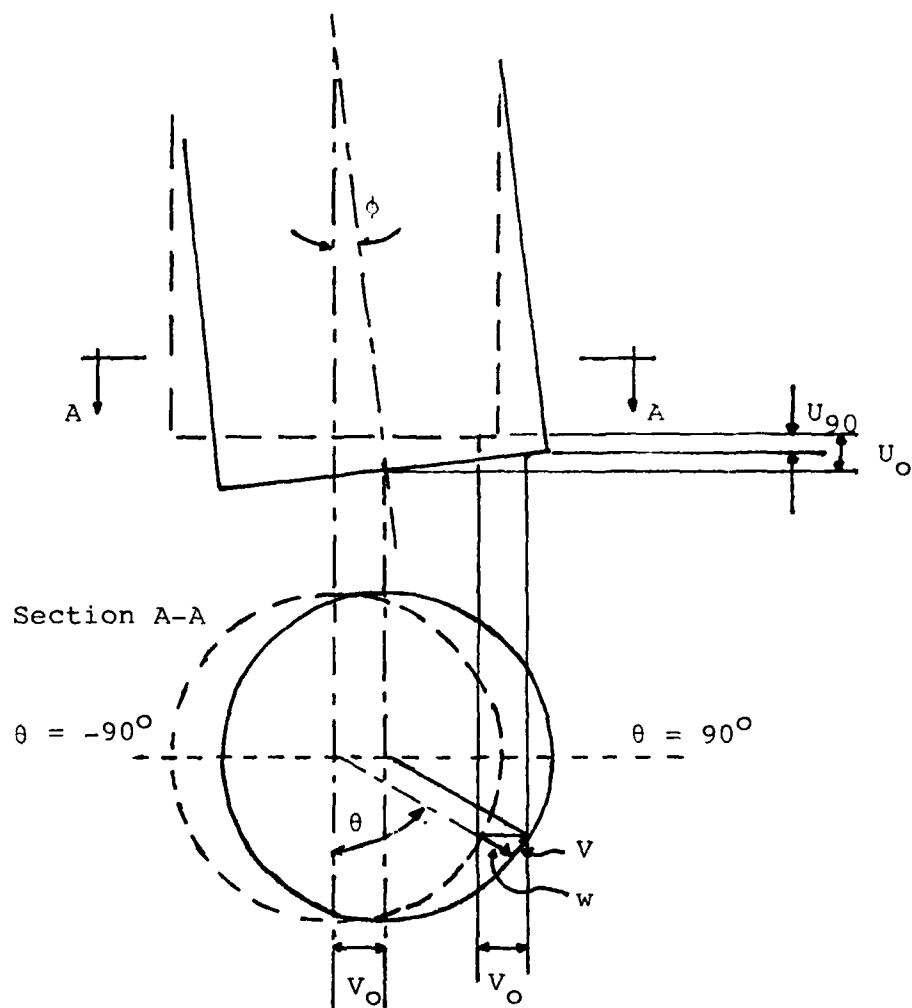


Figure 14. Displaced Free End From (29)

relevance. STAGSC has the ability to match boundaries along many connecting branches. In this case the boundary is not connected. However, the second branch is used to input the desired displacement. Skogh reads in the desired displacement u_3 via load data cards for the second branch. He then substitutes

$$u_{90} - u_0 = u_3 \quad (40)$$

into Eq 30; and along with the other two constraint Eqs 37, 38 forms the subroutine UCONST. UCONST allows the STAGS user to provide kinematic constraints in the displacement unknowns at internal and boundary points. The general constraint relation is of the form

$$\sum_i^N C_i V_i = 0 \quad (41)$$

where C_i are constants and V_i are the displacement components. What happens internally is that when the equations are being set up for the individual mesh points, at those points where UCONST is applicable Eq 41 has to be solved for also. The displacements are normally not fixed but rather have to meet certain kinematic relationships with surrounding points while the entire structure satisfies compatibility and equilibrium. This is the difference between using UCONST vs input boundary constraint cards, which form fixed positions. The dummy branch is used to internally impart the desired rotation. Therefore, by specifying the

top row as the place of interest in UCONST, the desired constraint equations are enforced with $u_{90} - u_0 = u_3$. The UCONST subroutine is listed in Appendix B.

A few points about the actual operation of the method.

1. The second dummy branch can be of any type, so the easier to model the better. I chose a 1 x 1 inch plate.

2. The specified displacement on this branch is in the x direction. Changing the sign on the input reverses the slope in UCONST and hence the applied rotation.

3. When trying to run a bifurcation analysis of the primary branch, STAGS will automatically run a bifurcation analysis of all branches and stop when the first convergence criteria is met for any branch; not all branches. Hence, to make sure that the bifurcation analysis is carried out on the branch of interest, the other branches should have their bifurcation analysis suppressed. This is accomplished by setting the variable L1N=1 on the I1 card for all the undesired branches. See Appendix B1 for an input card listing and the user's manual (Ref 5) for further guidance.

4. UCONST requires a do loop to set its way through all the mesh points. When the nodal size is changed in the circumferential mesh direction: the dimension, data, do loop, singularity check, and IY cards have to be updated in the UCONST subroutine as well as the number of constraint relations variable NCONST on the B1 card.

III. Modeling

Shell Model

Figure 15 denotes the pure bending rotation conventions. The -90° fibres are in a tension field whereas the $+90^\circ$ fibres are in a compression field. The radius R is 57.2958 inches. This facilitates measurements, since one inch on the circumference equates to one degree. The cut-outs are dashed indicating that they are not always there in my analyses. When they are, $2a = 12$ inches.

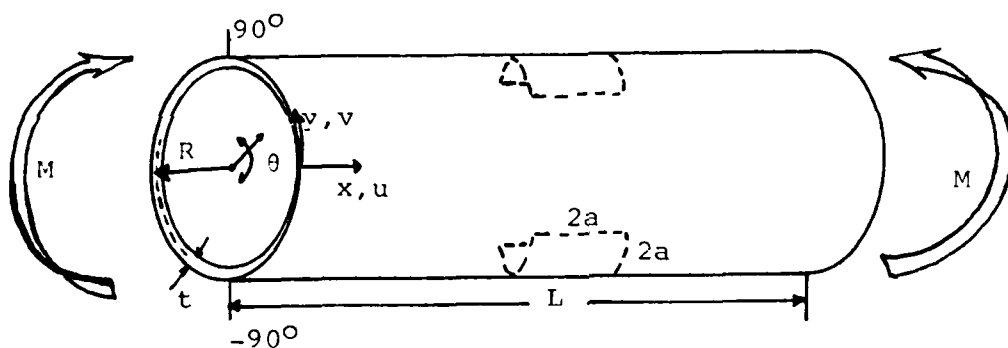
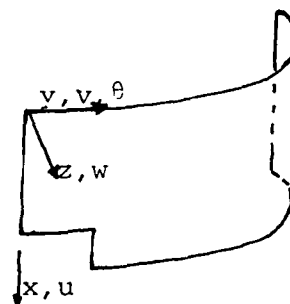
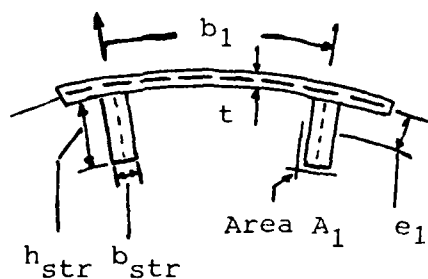
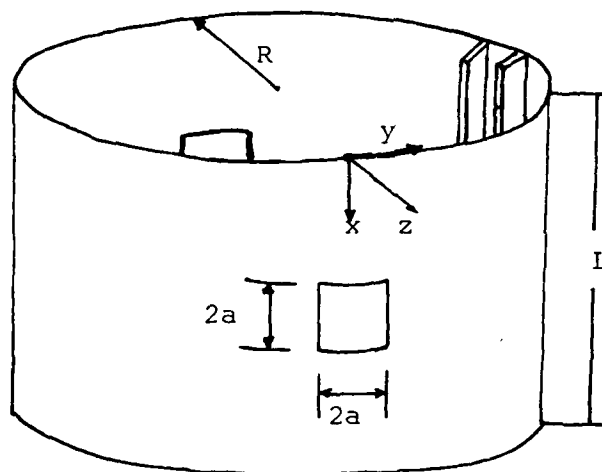


Figure 15. Pure Bending Rotation

Figure 16 is another view of the cylindrical shell. In addition, it has the stringer data drawn and tabulated. Palazotto (Ref 22) demonstrated nonlinearities due to cut-outs in stiffened shells were small even for a cutout size of $2a$ equal to $.3L$. To keep within that finding Nelson (Ref 21) used smaller cutouts when he studied shorter



$R=57.2958''$
 $t=.1''$
 $2a=12''$
 $b_1=3''$
 $b_{str}=.35''$
 $h_{str}=.8''$
 $e_1=+.45$
 $A_1=.28\text{in}^2$

$I_1=.01493\text{in}^4$
 $A_1/b_1t=.933$
 $I_1/b_1t^3=4.9767$
 $e_1/t=4.5$
 $E=10.4 \times 10^6\text{psi}$
 $\nu=.3333$
 $G=3.75 \times 10^6\text{psi}$
 $GJ=30302\text{in}^2$

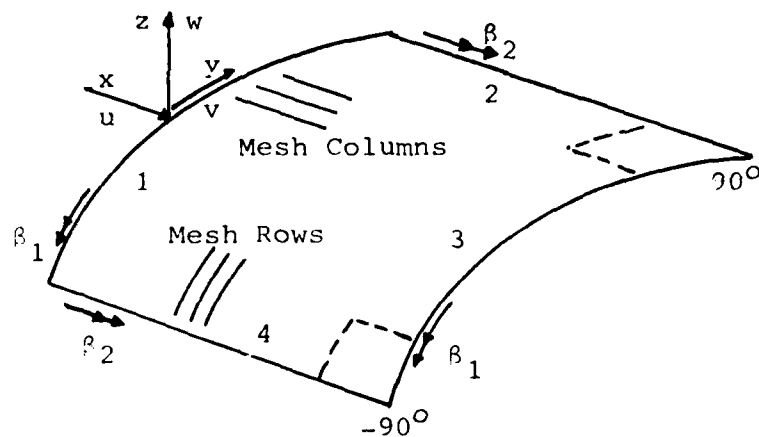
Figure 16. Shell, Stringer Geometry and Sign Conv.

cylinders. Since the major part of my work will be with an $L/R \geq 1$ range, I will also use the smaller cutouts.

The stringers placement followed that of Palazotto and Nelson. The three inch on center spacing with $\Lambda_1 = .28$ is well within the realm of smeared stiffener theory.

A significant effect of studying bending problems is that the moment takes away the third plane of symmetry due to loading asymmetry. It is not axisymmetric. So a quarter of the shell has to be analyzed each run. This doubles the nodal requirements for the same "fineness" of spacing which modeling one eighth of the cylinder allows for axial compression analysis. However, I am therefore able to study asymmetrical cutouts (one rather than two) without changing the modeling strategy. The boundary conditions are defined in Fig 17. Conditions of symmetry are imposed on boundaries 2, 3 and 4 throughout the analysis. The simple support boundary conditions, Eqs 26, presented earlier are imposed on the shell ends acting under axial compression along with the free condition for bending analysis. For axial compression runs, both line loads and displacements were imposed on the shell ends. For bending analysis, the dummy branch induced rotation is always used.

When building some runs for comparison with other published results, we noticed what has turned out to be an internal computational error in the STAGSC program. Figure 18 shows STAGS results for axial compression runs under displacement and force loading contrasted against Nelson's



BOUNDARY	PREBUCKLING	BUCKLING
1	Free, SS1	Free, SS3, SS4
2	Symmetry	Symmetry
3	Symmetry	Symmetry
4	Symmetry	Symmetry

Note: Symmetry means $u = \beta_1 = 0$ on lines 1 and 3
 $v = \beta_2 = 0$ on lines 2 and 4

Figure 17. Boundary Conditions for the Shell Model

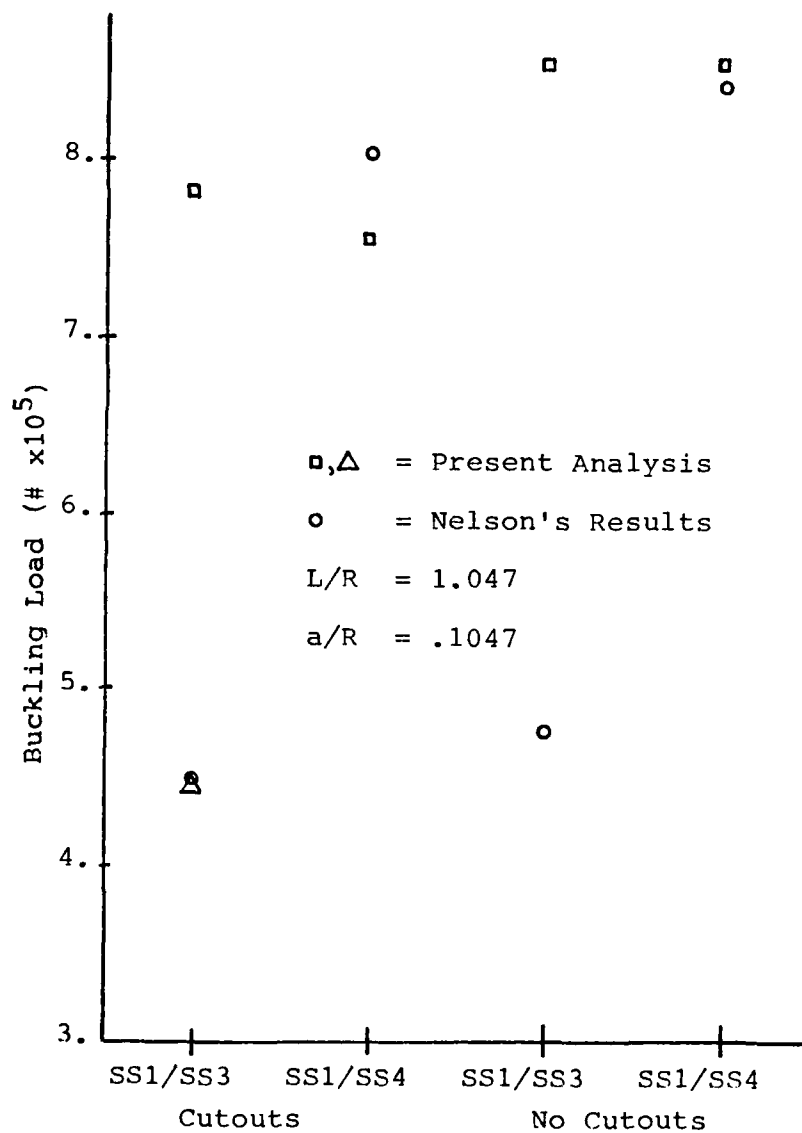


Figure 18. Comparison of Axial Compressive Failure Loads Under Force (SS4) and Displacement (SS3) Conditions

results. Data for stringer stiffened cylindrical shells with and without cutouts are examined. All Nelson's runs were made with displacement loading while the boundary conditions varied. The comparative results for SS4 conditions are reasonably close. It is when SS3 conditions are compared that a large disparity exists: around 450,000 for Nelson's vs 800,000 for present work. However, when force loading is introduced, Δ value for the SS3 cutout run, the results fall within 1% of each other. This has led to the conclusion that when the displacement loading is used with the STAGSC bifurcation option the stiffness matrix formed for the prebuckling boundary conditions is not decoupled from the buckling boundary conditions. When force loading is used this does not happen since a specific u has not been specified. When the force loading runs are made with SS4 boundary conditions, the same results are obtained as with the SS3 displacement combination. The first clue to the reason for these results came from the eigenvector printout sheet. For the displacement runs with SS3 conditions, the top row u values were zero which they shouldn't have been. This did not show up when force loading was used. Mr. Jörgen Skogh, Lockheed's STAGSC consultant and monitor, has been contacted about these findings.

This development has caused us to compare the bending moment results against the force SS4 combination axial compression results. Although the top row, boundary one condition, is set as free for the bending runs, we feel that

by setting in a definite rotation angle, the same thing is happening with the stiffness matrix. Results have shown this to be the case. Future work in this area with STAGSC should center around resolving this internal mathematical programming deficiency.

Finite Difference Mesh Arrangements

The grid systems developed for shell models with and without cutouts are illustrated in Appendix C. Since smeared theory is used in this study, a mesh line should be placed under each stringer in the circumferential direction. This necessitates a minimum of 61 nodes in the circumferential direction. Convergence studies were made with the results confirming the need for this arrangement in the compressive zone. However, there seems to be room for economy in the tension zone. A comparative bending run (Fig 19) with half the number of mesh lines, that is 6 inches apart, on the tension side was made with the same spacing as before on the compressive side. The buckling loads computed out to be the same but the eigenvectors were slightly different. More importantly, this was done on an unstiffened cylinder. Future studies will have to determine whether economies can be gained using this method. For this study, the mesh arrangement has remained symmetric about the middle column. Another point should be made here. Previous studies using STAGSA (Refs 15, 21, 22, 32) have used as a rule of thumb, 5 nodes per half sine wave in the eigen

analysis as a good measure for convergence. As was brought out earlier, STAGSA used a half station difference scheme whereas STAGSC uses a whole station method. Almroth (Ref 3) did converge comparisons between the two programs showing STAGSC to be much quicker and accurate. In fact, for similar accuracy we can use almost twice as large (sparser) grid spacing. This indicates that the smaller node count per half sine wave is allowable. However, you will want to be able to model the sinusoidal behavior accurately.

Since this analysis is concerned with the displacement effects of applying a pure rotation to the end of cylinder, an axial mesh spacing of 1" near the top boundary is used for all runs. The larger pertinent shape changes are seen to take place within the top 5 or 6 inches as was also indicated by Nelson (Ref 21). Stiffened cylinders generally buckle with one half sine wave in the axial direction. So spacing is determined more by economy and the desire to keep the mesh as square as possible. The 3" axial mesh spacing beneath the top 5 or 6 rows is entirely adequate. Unstiffened cylinders display more waves in the axial direction as discussed under background. The 3" axial spacing gives $2\frac{1}{2}$ nodes per half sine wave axially which I believe is sufficient for STAGSC analysis if the circumferential mesh spacing is "fine" (see Fig 19).

For the cutout region Palazotto (Ref 22) and Nelson (Ref 21) have shown that a mesh spacing of 1.5" extending

15" from the center of the cutout represent an optimum refinement as far as computer time vs accuracy is concerned. I will use this spacing strategy, as it also gives an additional mesh line between stringers circumferentially.

For the compressive analyses, I have used a combination of 1/8 shell and 1/4 shell models. The axial dimensions remain the same as discussed earlier. The circumferential dimensions mainly vary in the total length of the shell modeled; not the spacing between the node points. That is, for unstiffened axial compression, I ran runs with 15 by 31 spacing over 90° circumferentially about 15 by 61 spacing over 180° circumferentially. The total number of node points doubled but the spacing remained the same between them. This was done in a study of boundary condition effects. For the stiffened shells without cutouts, I kept the circumferential spacing the same as for the bending analysis: 61 columns over 180°. For the cutout analysis, I used 1/8 shell modeling as did Nelson (Ref 21).

IV. Results

Unstiffened Analyses

Short shells were originally chosen for our model analysis in order to stay away from the Brazier non linear effects. Also, previous work had been done (21, 22) on stiffened short cylinders with cutouts under axial compression against which comparisons could be made. Unstiffened cylinders were first examined to give us some experience with STAGSC.

Figure 19 is a plot of stress intensities for the maximum compressive zone at buckling for different mesh arrangements. The reasons for these grid dimensions were given in the modeling section. Models numbered 2, 3, 4, 6 and 7, shown in Appendix C, were used for these convergence tests. For axial compression analysis, the 15 x 31 mesh over 180° is too sparse. The buckling values obtained with it were 36% of classical. Keeping the axial mesh the same and halving the circumferential spacing gives results within 78% of classical. Again halving the circumferential spacing, that is doubling the node points in that direction to 121, the answer comes to within 95% of classical values. However, the total node point count of 1815 is very costly to solve. It was decided that the characteristics we were looking for in the unstiffened cylinders could be modeled adequately by the intermediate 15 by 61 mesh arrangements. Also, as is seen later on, for stiffened shells (Fig 28) this same grid spacing gives very good results.

Figure 19 shows the circumferential and axial node point counts per half sine wave for the respective mesh arrangements. As the circumferential spacing became "finer" (more mesh lines per direction) the node point count rose accordingly. For 121 mesh lines we get 6 node points per $\frac{1}{2}$ sine wave. It is interesting that for a given axial spacing the convergence is shown to be a function of the circumferential spacing. This means that the axial spacing has to be at least a certain minimum to model the cylinder adequately. There has to be enough grid points to let the equations model the shells stiffness correctly. However, it seems that a lack of mesh lines in one direction can be compensated for, up to a point, by increasing the lines in the other direction. The best practice is to keep the grid sizing as square as possible with as fine a mesh spacing as is economically feasible.

Also, mesh spacing strategy usually starts with a large grid spacing, then decreases the spacing around regions of interest. This method was used in this thesis, by having 1 grid line per inch near the top boundary where the loading is applied, and $1\frac{1}{2}$ inch spacing around the cutouts. However, this was done to study the deflections and stresses in these regions, not to get a better buckling convergence. As was mentioned earlier, for bending analyses, only the side of the cylinder under the compressive zone is of buckling interest. Figure 19 shows that a mesh arrangement (model 6) with half the mesh lines in the tension zone, can give the

same results for bending analyses as symmetrical arrangements. This was only tested for unstiffened cylinders; further studies will have to investigate this mesh strategy for stiffened cylinders where common usage says there should be at least one grid line under each stiffener. For all the axial compression vs end rotation loading analyses in this thesis, the circumferential grid spacing was symmetrical about the middle column.

The major finding of this thesis can be seen in Figs 20, 25, 26 and 27. Looking first at unstiffened short cylinders (Fig 20) under pure bending, via kinematic end rotation constraints, the prebuckling deflection shapes do not follow what is normally called "beam bending" deflection. That is, instead of the cylinder deflecting as pure body motion with the corresponding convex shape, the cylinder deforms as shown in Fig 20. This figure details only the top half of the cylinder with the bottom half being a mirror image. There isn't enough material in these short unstiffened cylinders to allow the stress loading caused by the applied end rotation, to dissipate through flexure type deflections. Another way of saying it is that the cylinder isn't stiff enough to counteract the local end moments M_x which cause a shear strain type deformation. By keeping the end plane undistorted the material around -90° is put under pure tension; whereas, the fibers around $+90^\circ$ are subjected to pure compression. The resulting deformation has the material on the tension side necking in, and the

material on the compression side bulging out. The maximum extent of the inward deformation or outward bulge is labeled MWD (on Fig 20). Also on this figure, the V deflection at the middle column is sketched. This line is seen to take the shape normally associated with bending. This indicates that the vertical plane through 0° and 180° about which the end rotation is applied does deflect in the "normal manner". Figure 21 is a top view of the first few rows of the cylinder. It shows how the deformations vary around the circumference increasing to a maximum at row 5 (4" down). At 0° and 180° there is a very slight motion (not discernible in this plot) towards the bottom of the page.

It should be mentioned at this point that the actual deflections are of order 10^{-3} inch with an L/R ratio of 1.047. So, this effect would not be discernible to the naked eye.

Again looking at Fig 20, the inward/outward deflections in the tension and compressive zones respectively do not get back to the original circumference position. This changes when the L/R is doubled to 2.09 where the form takes on the shape designated in Figs 22 and 23. The length of cylinder is doubled keeping the radius the same while the applied end rotation angle is kept constant. The result is that the deformations now cross over the original circumferential position and start to assume flexure deflection type displacements at the mid section. This transfer region is called the crossover point (CP) and is designated in Fig 22. As

the length to radius ratio increases for the same applied input rotation, the deformation effects diminished in magnitude as well as position along the length of the cylinder. Figure 22 shows that as the L/R ratio approaches 20 the effects disappear. In fact, for L/R ratios greater than 6 the effects can be said to be negligible. This is still well below the L/R value of 50 where the Brazier effect starts to take place. Figure 23 is a plot of the W deflection vs V deflection at the mid section as the L/R varies. Since the V deflection of the middle column has been shown to follow "beam type" flexure, the relation of the W deflection at the end columns to V gives a good indication of the cylinders behavior. As is seen in Fig 23, the ratio is almost unity at L/R equal to 20 and for all practical purposes can be considered as such for L/R ratios greater than 6.

A final comment about using the pure bending loading method; all motion degrees of freedom are accounted for with respect to free body motion through the symmetric conditions on boundaries 2, 3, and 4 except for translation in the $-90^\circ/90^\circ$ plane. Some restriction must be added in the program to stop this from occurring. A restriction of setting V equal to 0 at the middle column of row 1 was used. This was chosen, rather than restricting V at the center, since the end plane rotation is the applied loading method. The V restriction at the center would lead to the same results but the ends would be deflected rather than the

center. Also, the V restriction is preferable over a W restriction at the -90° or 90° columns since V restricts in-plane motion; whereas, the W would restrict motion normal to the surface which is much weaker.

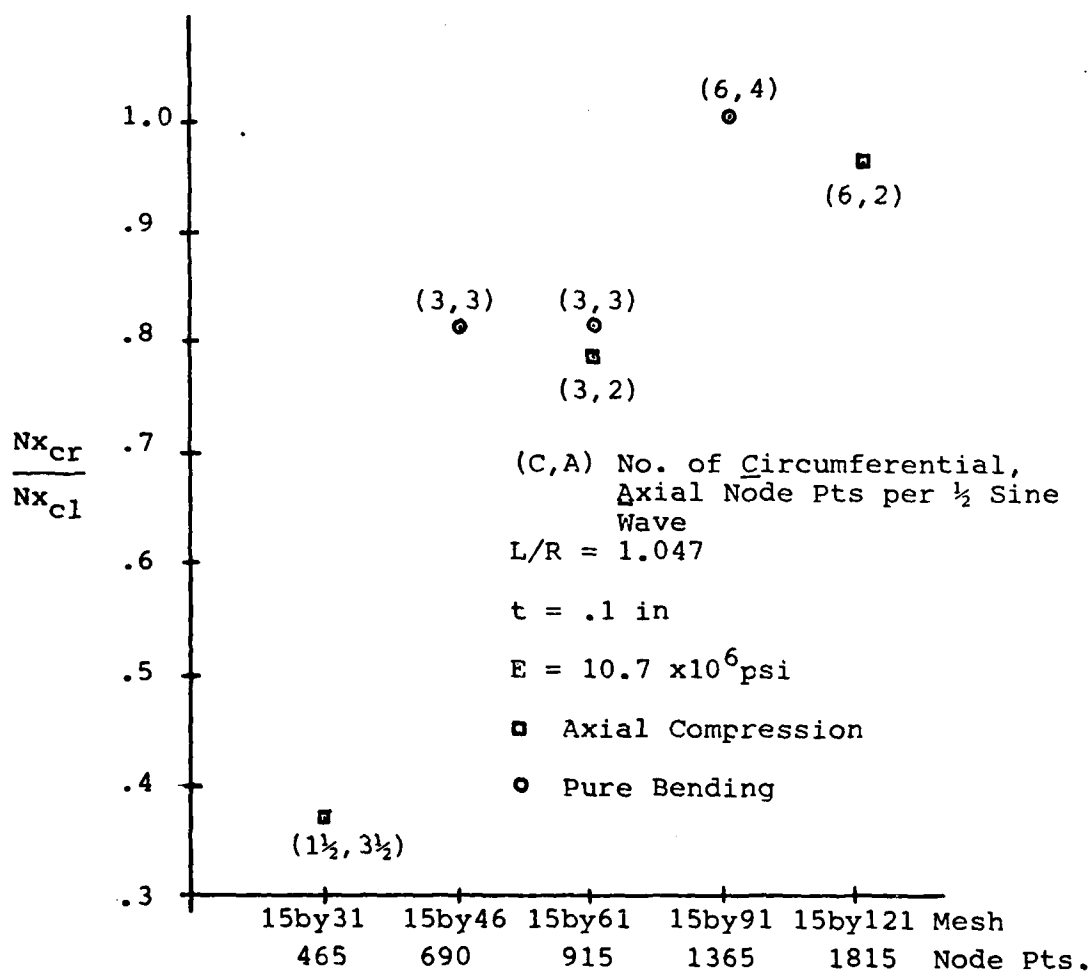


Figure 19. Buckling Stress Intensities vs Mesh Size
 For Pure Bending and Axial Compression of
 an Unstiffened Cylinder

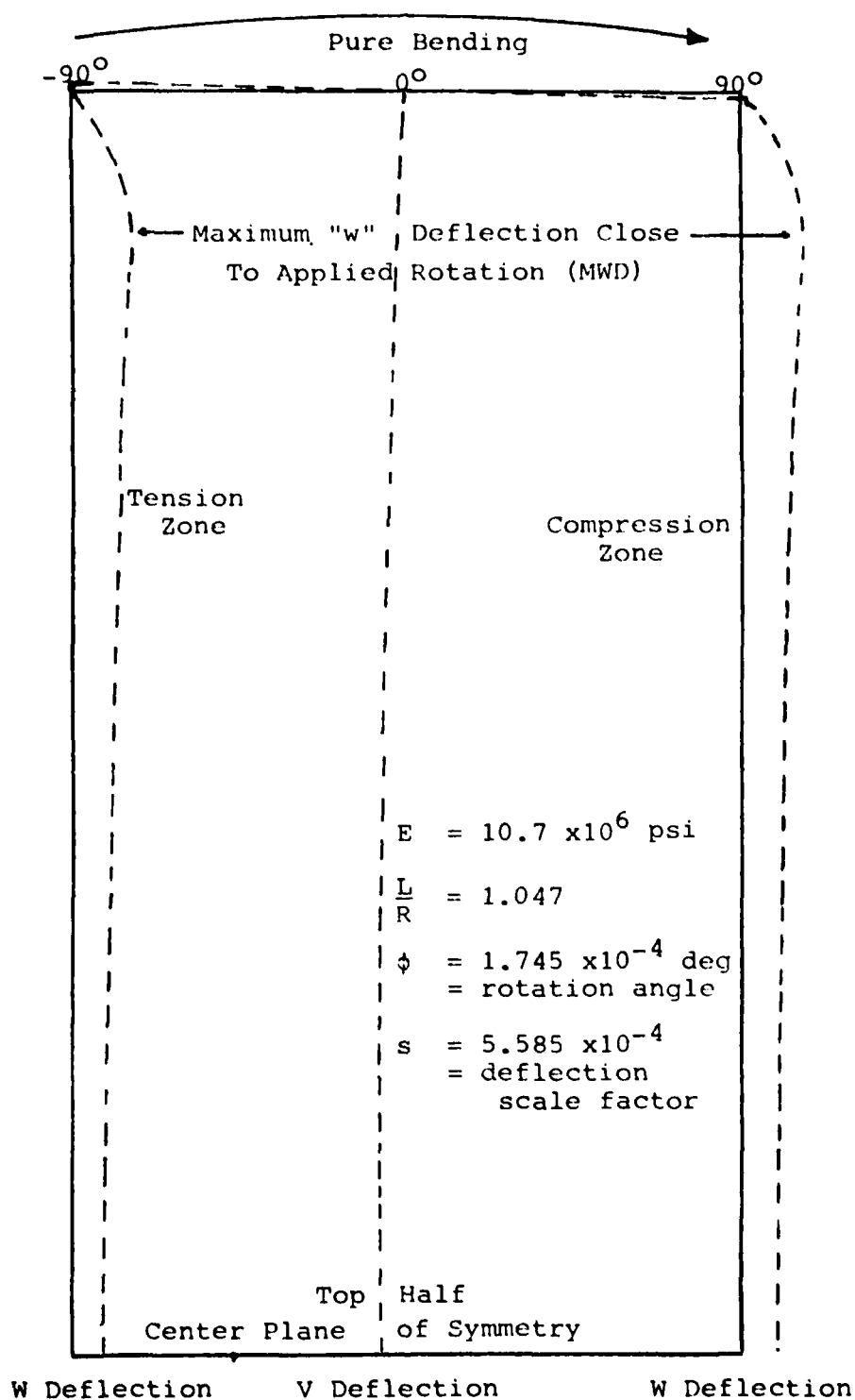


Figure 20. Prebuckling Deflections For Unstiffened Cylinder

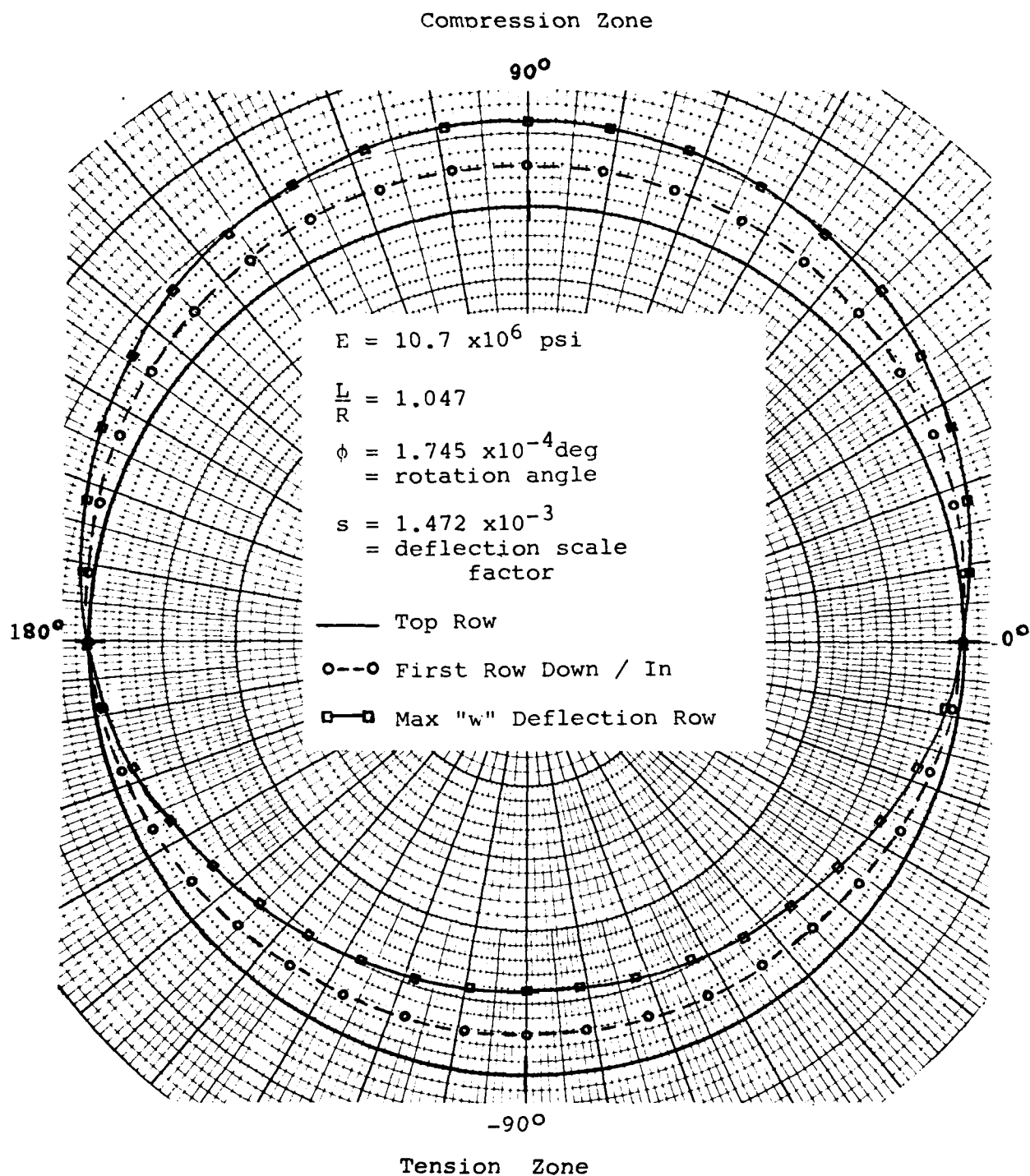


Figure 21. Top View of an Unstiffened Cylinder Under Pure Bending

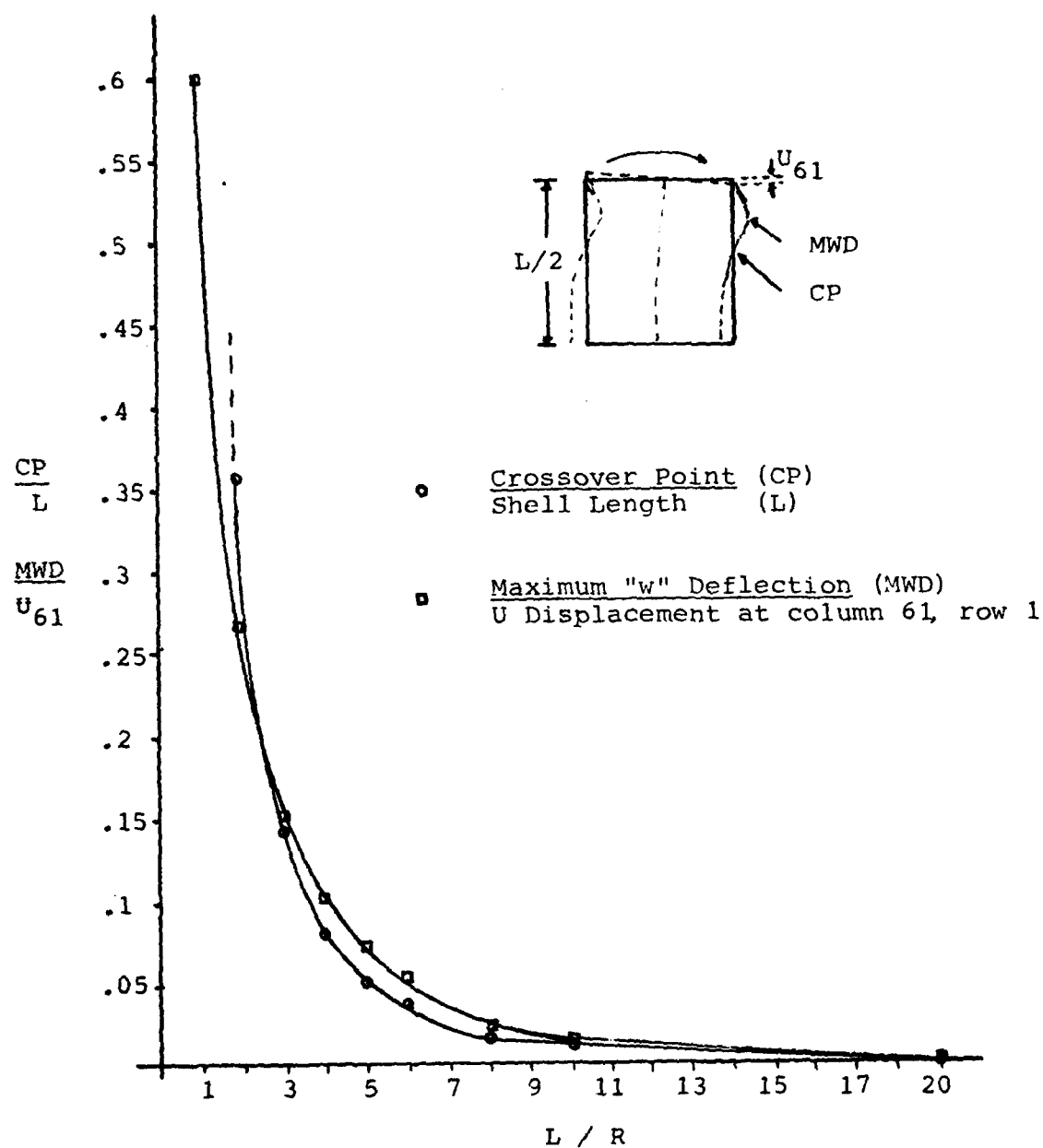


Figure 22. Length to Radius Effects For an Unstiffened Cylinder With an Applied End Rotation

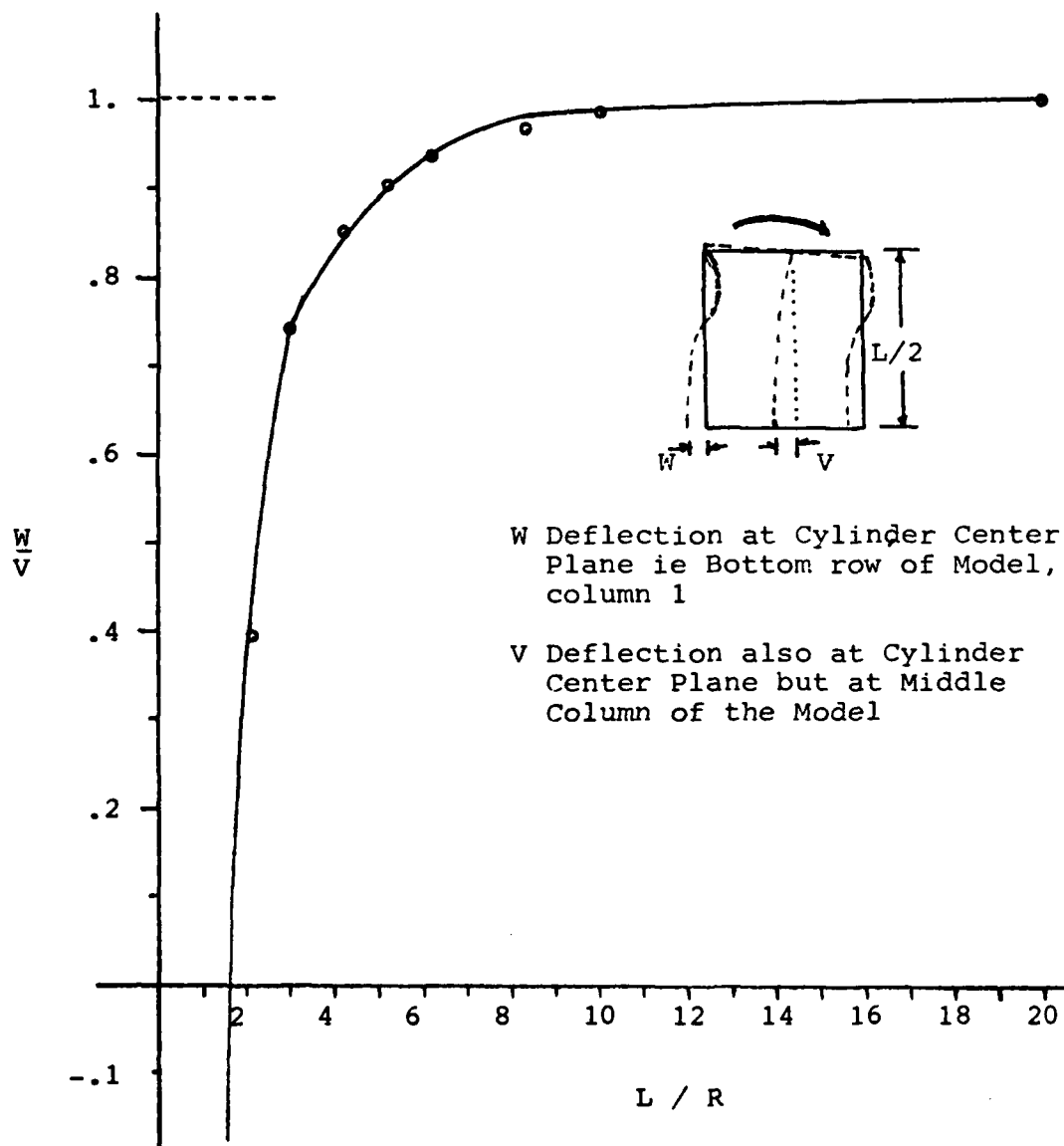


Figure 23 W vs V Deflection for Given L/R Ratios of an Unstiffened Cylinder With an Applied End Rotation

End Ring Stiffened Shells

Since the unstiffened cylinders were not able to resist the deformations caused by the end plane bending rotation, a study using discrete rings positioned near the ends was undertaken. Figure 24 is a plot of the results for the first 7 rows of the compression column at 90° . It is seen immediately that for the ring configurations chosen, the basic deformation pattern does not change.

One ring added at the top row, whether internal or external, has no effect. It acts like a point mass and does not affect the axial bending stresses. Rings added at row 2 (1") or row 3 (2") do affect the initial slope and specific shape of the deformation pattern but do not alter the overall characteristics. If the ring's size is doubled and placed closer to the MWD (row 3), the maximum deflection is delayed and somewhat reduced, but not appreciably. Therefore, it is indicated that the cylinder wall is still the primary resistance medium, and that the rings used are ineffective for controlling initial deformations. A further parameter study varying the ring's cross sectional area, moment of inertia, and placement could better define the rings effectiveness.

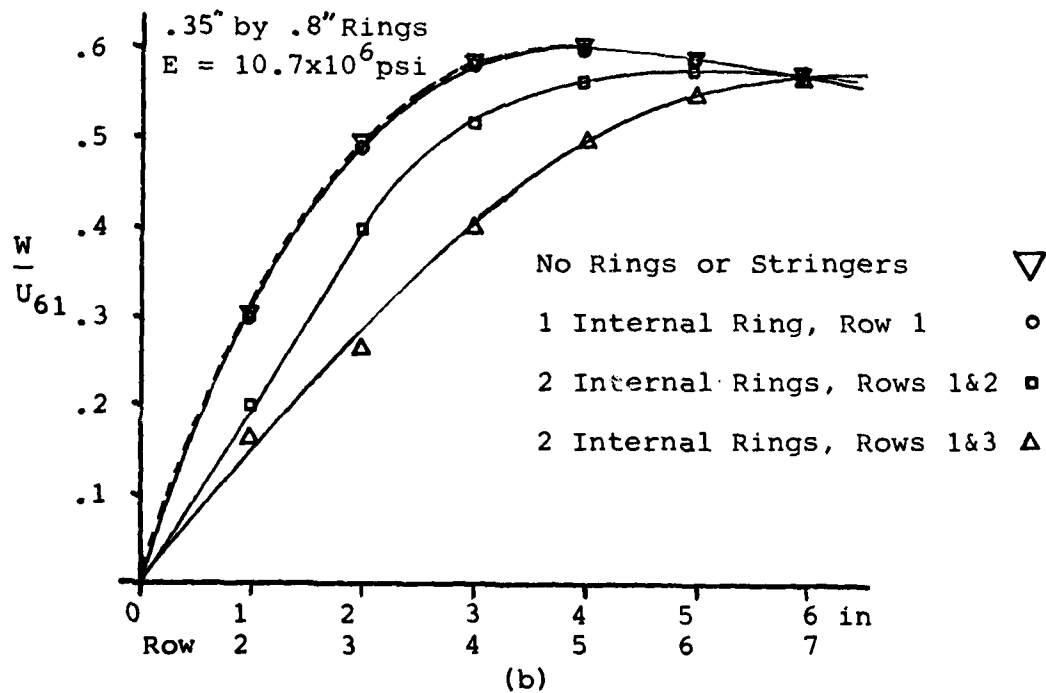
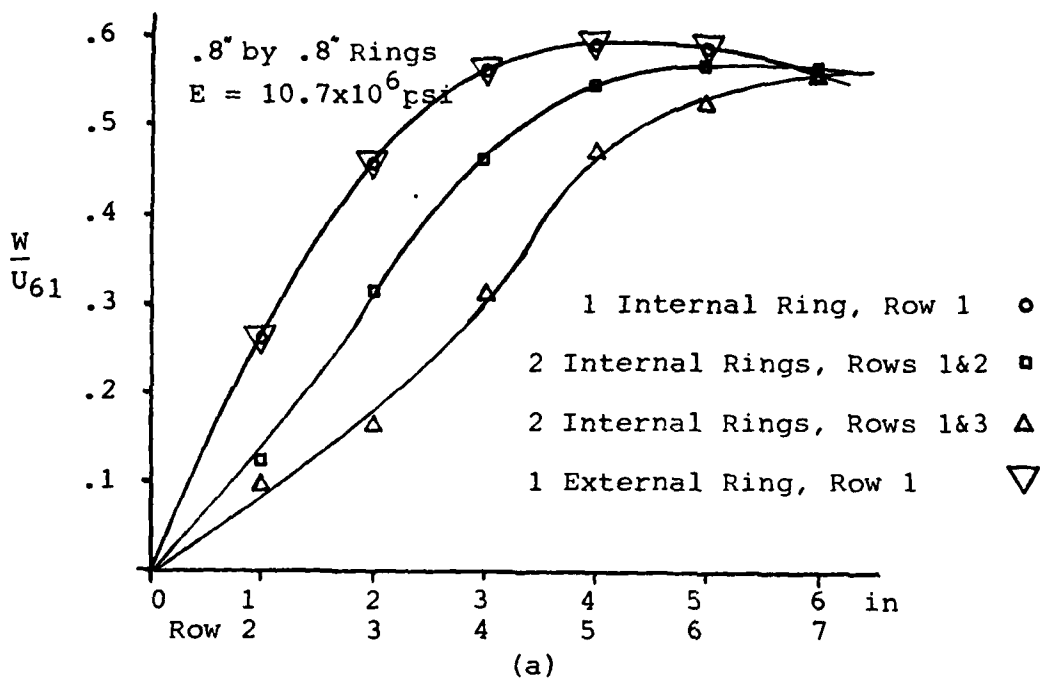


Figure 24. The Effect of Ring Stiffening on Pure Bending Induced Displacements

Stringer Stiffened Shells - With and Without Cutouts

When internal stringers are added to the cylinder, the initial deformation pattern changes. Figure 25 depicts a cylinder with internal stringers positioned 3" on center, studied using smeared theory. The cylinder/stiffness combination is now able to resist the end moments caused by the bending rotation of the end plane. In effect, the smeared stringers have made the shell wall thicker, more able to act like a column. However, the shell is still too short to allow for complete flexure analysis. There is not enough distance between the end constraints. On the compression side, the stiffened cylinders follow the compression zone radial deflection as described by (21). The tension side deforms with the same shape, not the mirror reverse as it would be with total compression loading. The figure again has a crossover point which should become negligible with an increase in the L/R ratio. A study similar to Figs 22 and 23 was not completed, but it can be surmised that the same effects would develop; probably faster since the shell is stiffer. Model numbers 1, 3, 5 in Appendix C were used in a L/R study from .698 to 1.361 to contrast results against stiffened cylinders with cutouts.

Figures 26 and 27 depict cylinders with 1 asymmetrical and 2 symmetrical cutouts respectively. As can be seen, the cutouts affect the prebuckling deformation patterns. In both types, the cutouts cause a commensurate loss in strength

which lets the deformations above the cutout progress as if there was little restraint. The initial deformations close to the top row follow that of the stiffened shell without cutouts, although the MWD value is 65% less. However, there is no crossover point anymore. The cutout(s) at the center of the cylinder lets the stresses redistribute to areas at the sides of the cutout. The bending restraints, which forces the crossover to satisfy compatibility relations, has been altered due to the missing section. Hence, the dotted depiction of the deflection over the cutouts assumes almost a linear relationship. Model numbers 16, 18, and 20 in Appendix C, are used for axial compression analysis. The circumferential extent is 90 degrees but symmetry allows the full 180° to be modeled. However, this lets us only examine the case of two cutouts under axial compression. For bending, model numbers 17, 19 and 21 A & B, are used. Minor input card changes in the subroutine wall allow us to consider either one (B) or two cutouts (A) respectively.

The stiffened cylinders were loaded with the same bending rotation angle as was used for the unstiffened analyses. The stress intensity at the 90° column (maximum compression column) of row 1 at buckling was contrasted against the same value under axial compression. Figure 28 depicts the results. The general movement for the entire graph is progressively higher with increasing L/R. This implies that the buckling loads increase with length. However, my analysis runs were for limited changes of length

of short cylinders. Nelson (21) plotted the same progressive movement for SS4 boundary conditions but went on to show that for a greater L/R ratio equal to 1.78 the graph drops down again to below the values for $L/R = .698$. The pertinent mechanism at work is the interaction of the SS4 boundary condition with the short shell. Nelson shows that for other simple support (SS1, SS3) boundary restraints, the plot remains close to horizontal. As was brought out earlier in the shell model section, we are required to use the SS4 boundary support for analysis, due to STAGSC handling of displacement loaded buckling analyses. Pure bending rotation is a form of displacement loading. Therefore, this boundary condition will affect the comparison between axial and rotation loading analyses.

For stiffened cylinders without cutouts, Fig 28 shows that the bending critical values are above the axial compression loaded values and tend to diverge slightly as the L/R ratio increases. An explanation for this behavior, involves crossover point analysis under prebuckling displacement rotations. As was pointed out earlier, an internally stringer stiffened cylinder deforms in the shape of Fig 25. When axial compression is compared with the shape for the same L/R, the axial displacement pattern at 90^0 follows the same concave/convex arrangement. However, the crossover point is closer to the top edge for the axially compressed cylinder. The variation is probably due to the effect of stringer eccentricity aiding the initial defor-

formation under bending and resisting the return mechanism. The difference in crossover points causes a commensurate change in the effective length (distance between the cylinder top half and bottom half crossover points) between the axial and bending loaded models. Since the bending effective lengths are smaller in each case, their buckling loads are slightly higher. This effective length difference increases slightly with an L/R increase which causes the divergence. These effects are associated with short shells only; as soon as "beam type" flexure predominates, the stress analysis models change. However, for these cases the maximum difference was less than 13%. Therefore bending buckling stresses can be modeled by axial compression analysis to within that percentage tolerance for the given L/R ratios.

The picture changes when cutouts are introduced. Now there is less material under both loading schemes and the buckling intensities are lower for all L/R ratios compared with no cutout cylinders. Further, the maximum bending loads have less material to average over and consequently the cylinder buckles earlier when compared against axial compression analysis. Although the SS4 boundary condition is still present, the cutout condition is now dominant. But, as the shell length increases, the hole (size held constant) effect diminishes in importance and the critical axial vs bending intensity values converge between themselves and the no cutout values.

Two other points can be made from Fig 28. First, there is negligible difference between the one cutout and two cutout models under bending loading. The critical N_x values are within .1% of each and therefore plotted together. This effect is also clearly demonstrated on Fig 32 where the one cutout and two cutout stress intensity flow lines lie right beside each other. The reason for the unimportance of the other cutout is that it lies in the tension zone, which does not contribute to the maximum compression fiber analysis. Second, a "finer" mesh (15 x 121) is plotted on the figure for axial compression analysis of a stiffened cylinder without cutouts. For unstiffened cylinders, increasing the mesh from 15 x 61 to 15 by 121 resulted in a buckling load increase of 19%. For stiffened cylinders, this same mesh refinement only brings out an increase of 5.8%. This indicates that for stiffened analysis a moderate spacing models the cylinder very well. This was the justification for using the 15 x 61 mesh arrangement as the primary strategy.

Figure 29 depicts the critical bending moment values for the different cutout and no cutout cylinder models as the length is changed. The algorithm used to calculate the moment is given in Appendix B. Since the cylinder is loaded by specifying a rotation angle, the applied moment is found as a by product from the resulting N_x values. The SS4 boundary condition again causes the rise in the critical moment value as the L/R ratio increases for these

short cylinders. What is interesting is the closeness of the different critical moment values for the shell cylinder models in question for each L/R ratio. This indicates that we are able to predict critical moment cutout values using no cutout model analyses. The maximum difference lies within 9% for the L/R range studied. There is some difference between the one cutout and two cutout values which arises from using the top row N_x values for the total model to calculate the total moment. However, this difference is always less than 9%.

Plots of the eigenvectors for the no cutout and symmetrical cutout stiffened cylinder models are given in figures 30 and 31 respectively. These figures are included to show that the circumferential buckling mode shape under end rotation loading doesn't change with the addition of a cutout. The axial compression loading mode shapes change but only in the relative magnitude of displacements. For all cases, the wave lengths are the same, giving approximately 12 half sine waves per 180° compression. The axial wave form for both the cutout and non cutout stiffened models is one $\frac{1}{2}$ sine wave, with the maximum normalized deflection occurring at the center of the shell. This is contrasted with unstiffened cylinders which have many half sine waves in the axial direction.

An attempt was made to correlate the cutout model loading under axial compression to that under pure end bending by means of a ratio depicted in Fig 33. The

approach was motivated by the convergence of the bending vs axial values in Fig 28 and the equal number of $\frac{1}{2}$ sine waves over the cutout for the different loading schemes. Figure 31. It was felt that the total load above the cutout could be used as a predictive technique. The total load above the cutout for both loading schemes was arrived at by: 1. Multiplying each top row prebuckling N_x value above the cutout by the distance it works over. 2. Multiplying each of the above values by the eigenvalue at buckling. 3. Summing the values. These total loads were then used in the ratio in Fig 33 and graphed. The result was a plot that decreased as the length increased which was expected due to the convergence of Fig 28 points. Expected values for bending buckling loads above a cutout can be obtained using these ratio values, especially for $L/R > 1$.

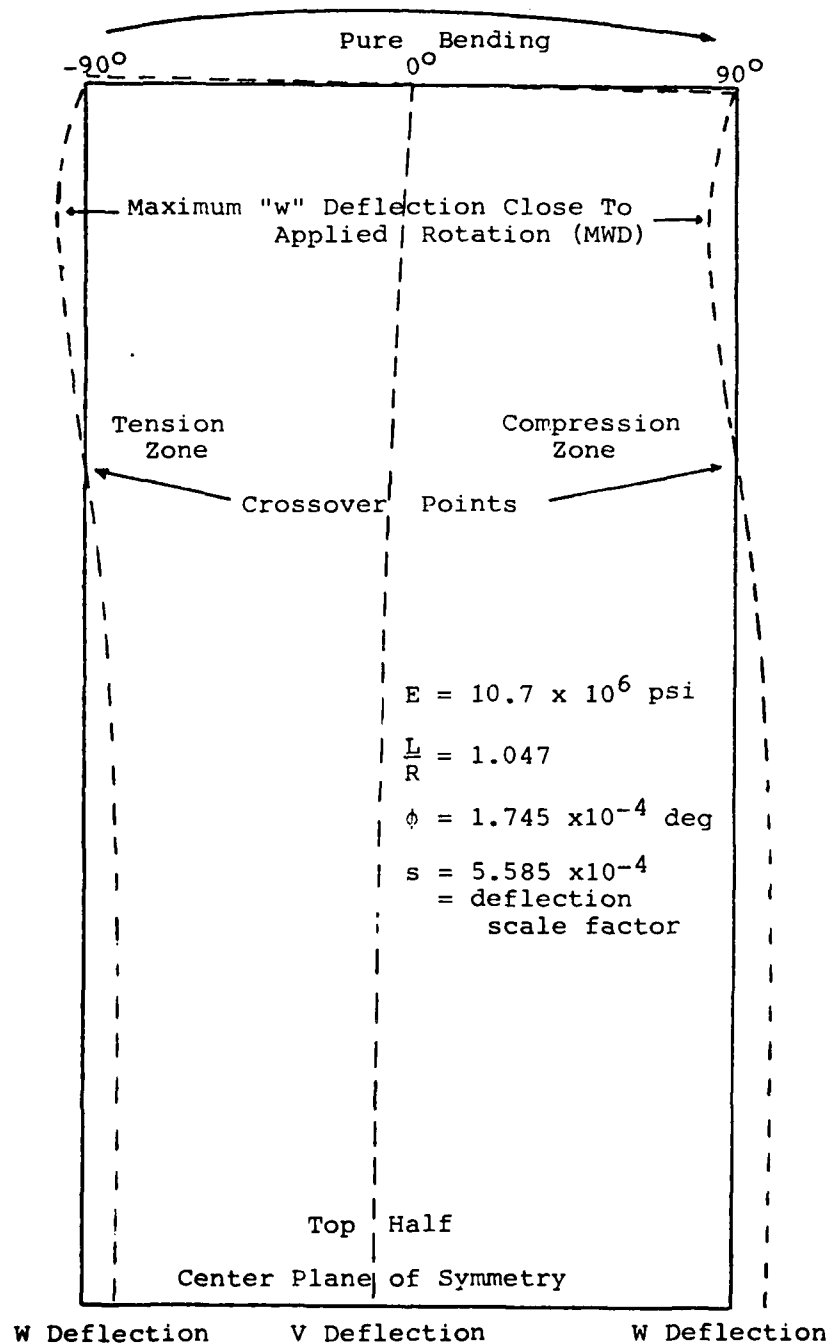


Figure 25. Prebuckling Deflections for Stiffened Cylinder

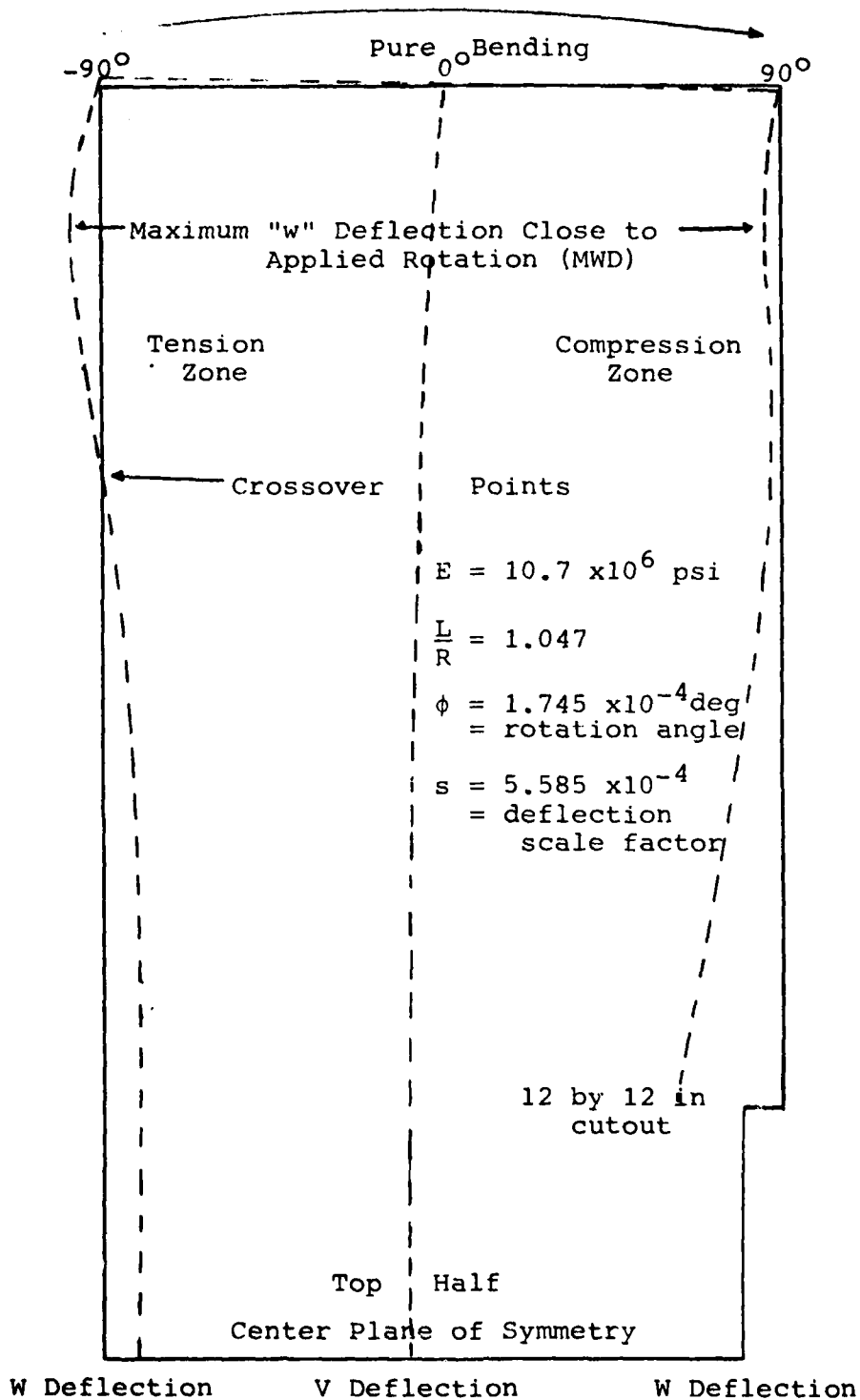


Figure 26. Prebuckling Deflections for Stringer Stiffened Cylinder With 1 Cutout

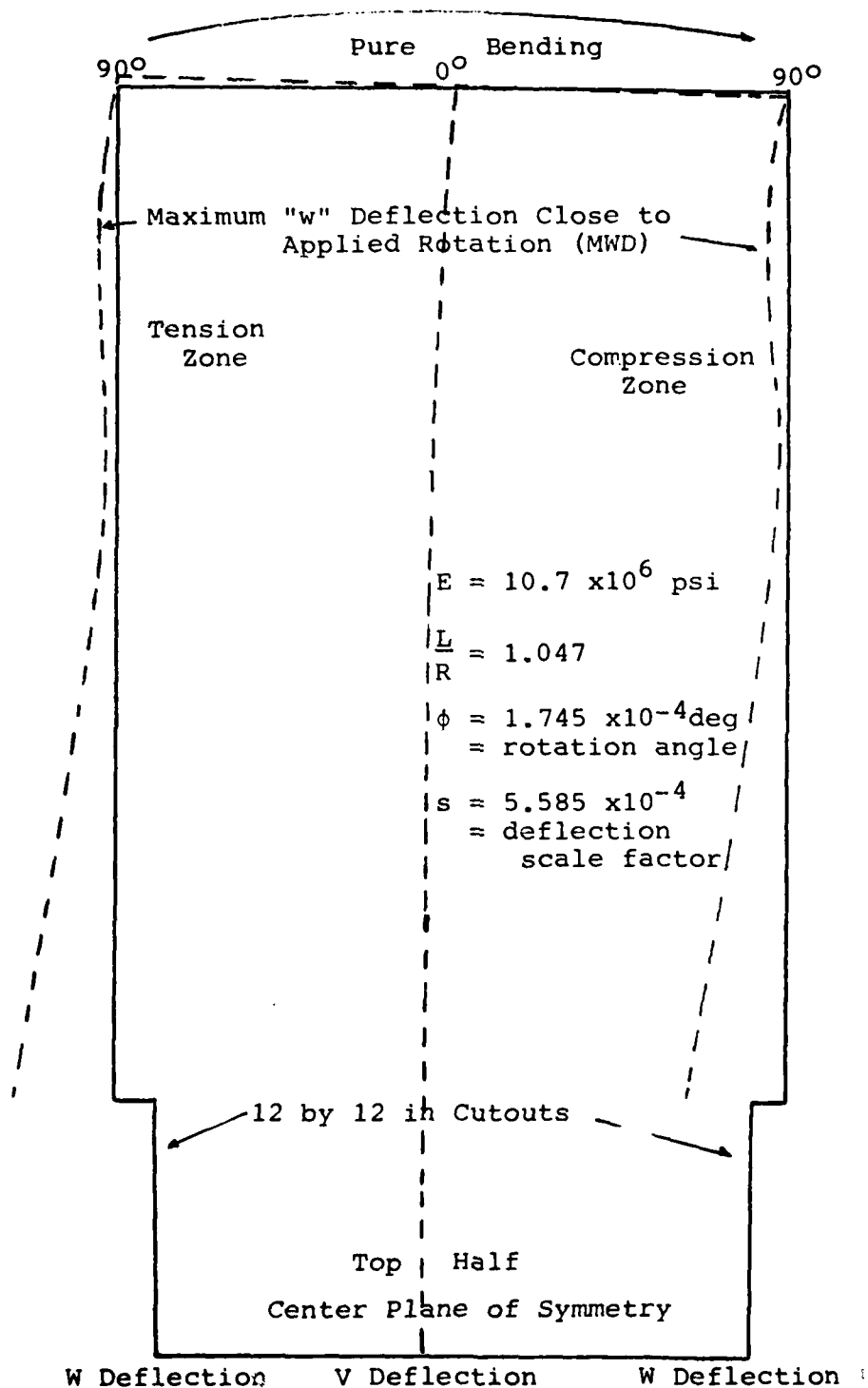


Figure 27. Prebuckling Deflections For Stringer Stiffened Cylinder With 2 Cutouts

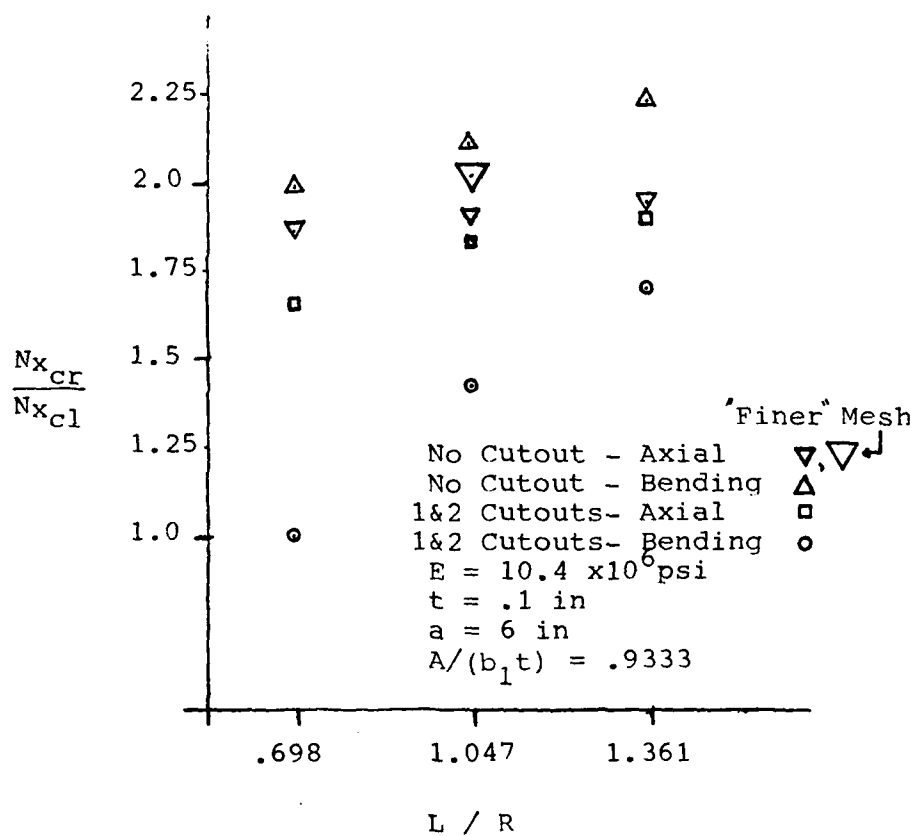


Figure 28. Axial Compression vs Pure End
 Rotation Buckling Stress Intensities
 For Stiffened Cylinders With and
 Without Cutouts

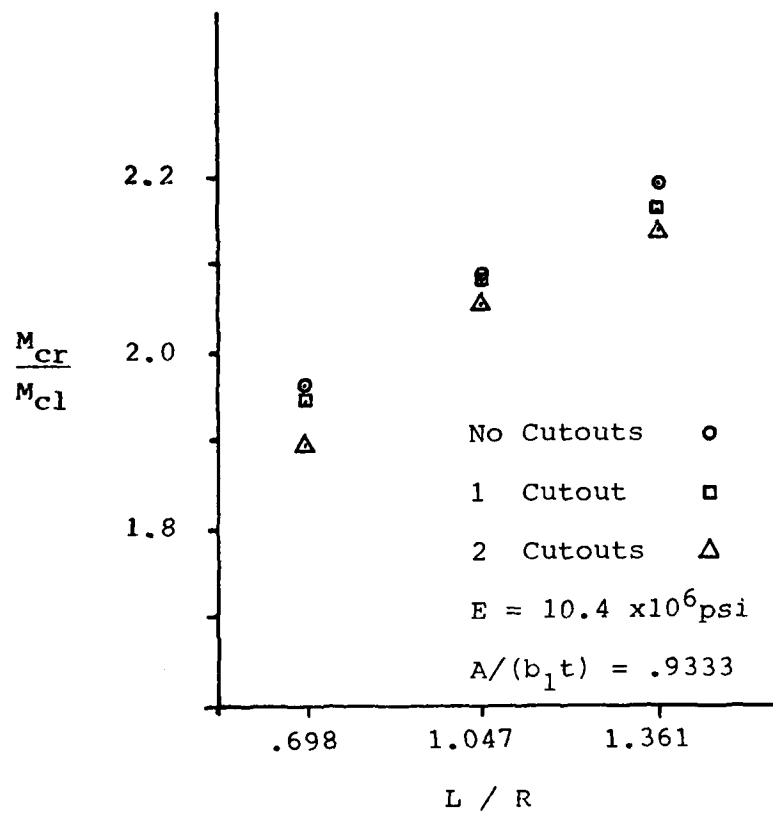


Figure 29. Buckling Moment vs Length For Stiffened Cylinders With and Without Cutouts Under Pure End Rotation

Compression Half

$x = 30.0$ " Middle Row Which Separates
Top From Bottom Half of Cylinder

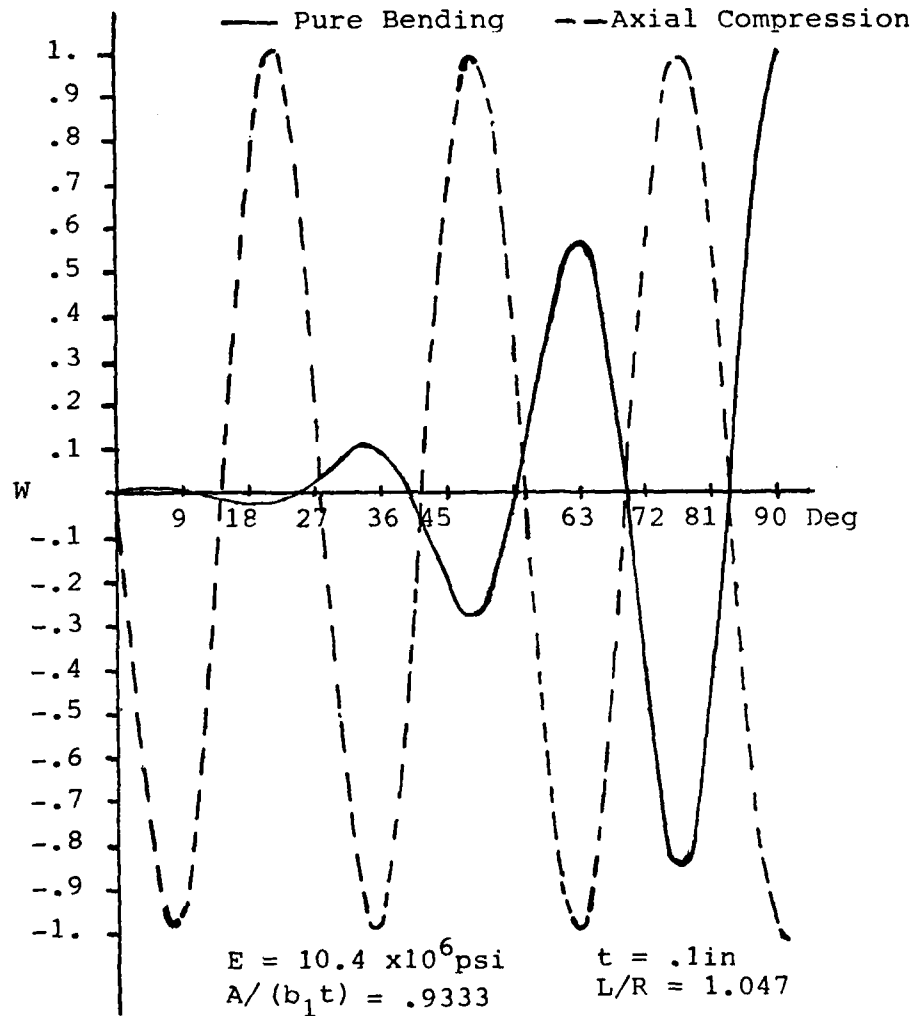


Figure 30. Eigenvectors For Axial Compression
and Pure Bending Loading of a
Stiffened Cylinder

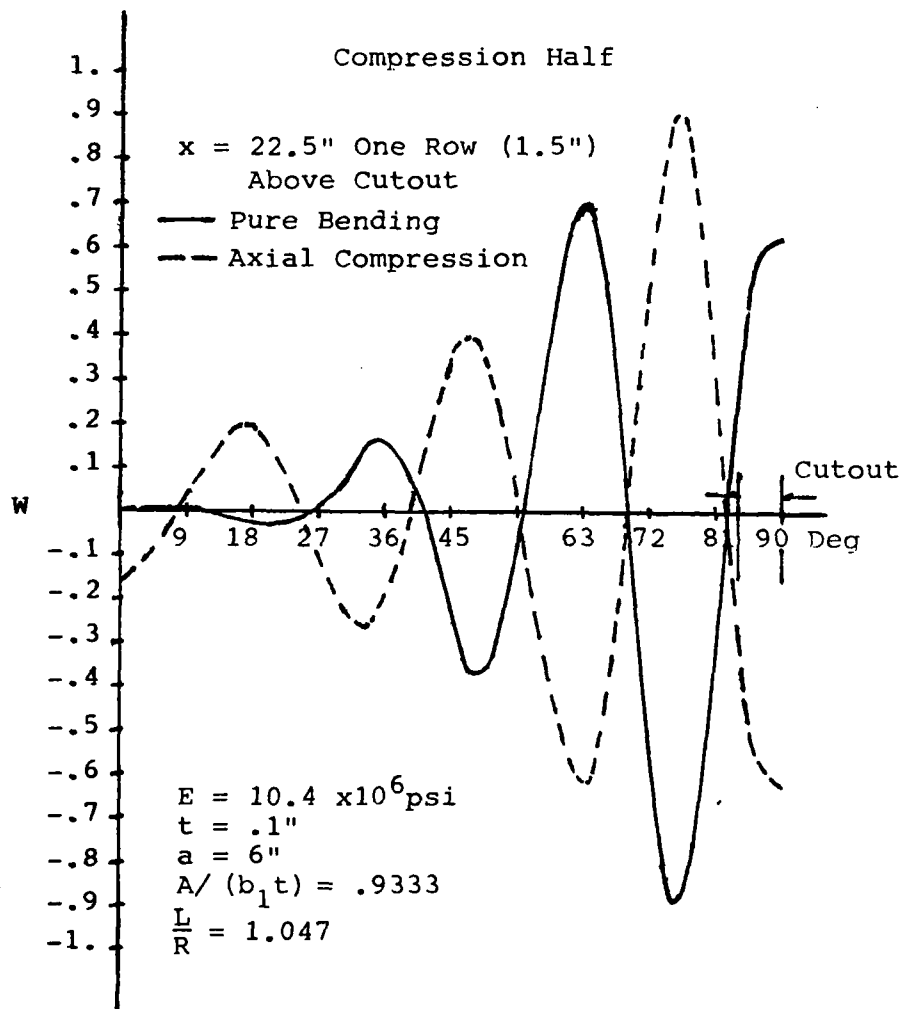


Figure 31. Eigenvectors For Axial Compression and Pure Bending Loading of a Stiffened Cylinder With 2 Symmetrical Cutouts

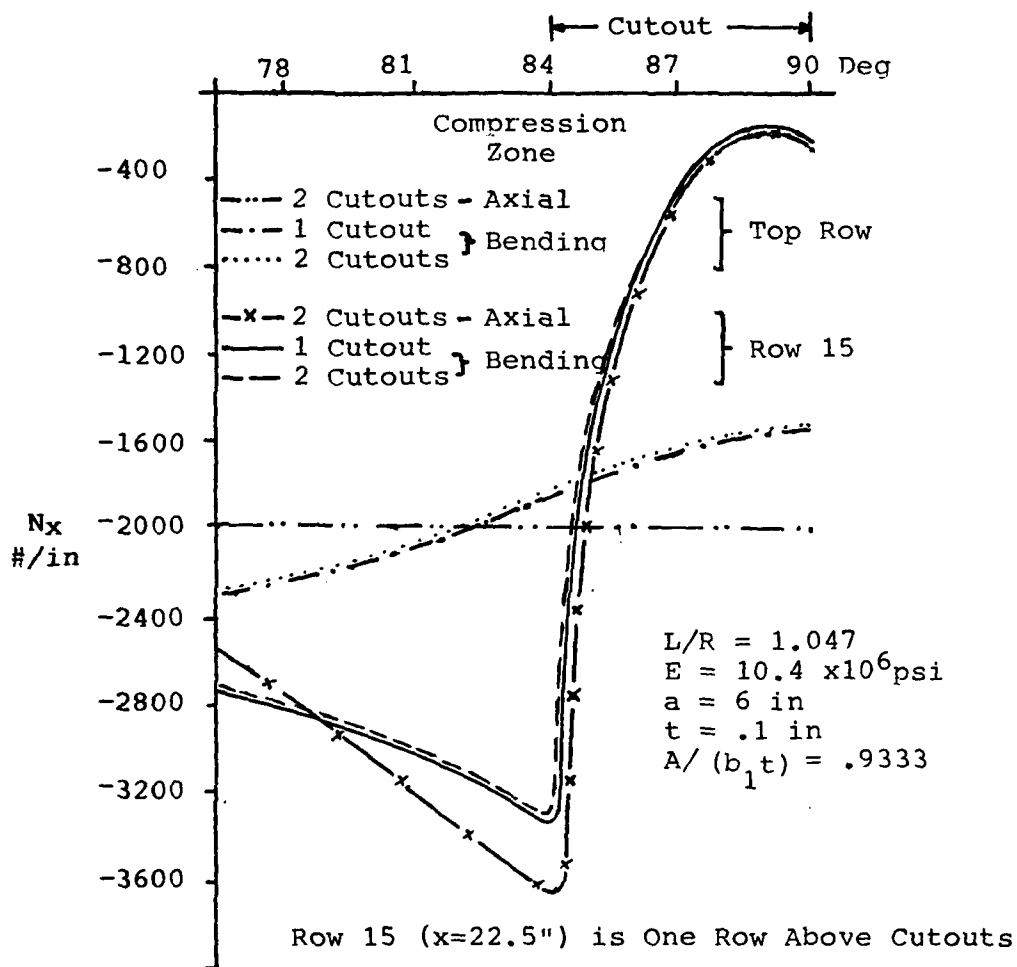
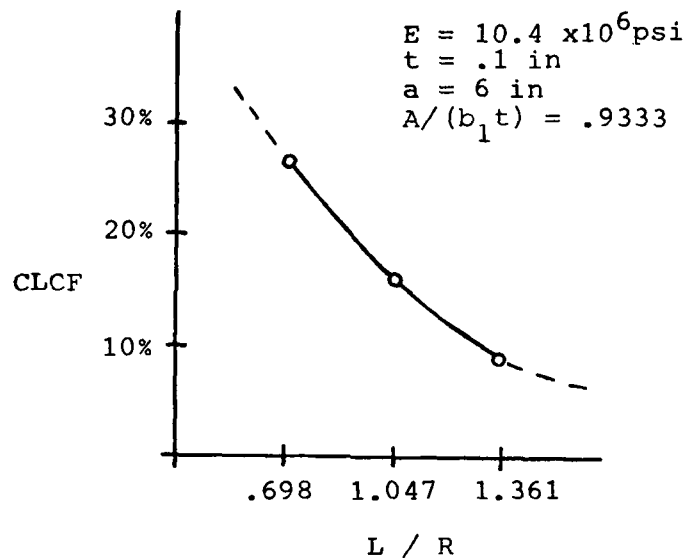


Figure 32. Stress Intensity Flow For Axial Compression and Pure Bending Loading of a Stiffened Cylinder at Buckling



Where the Critical Load Cutout Factor (CLCF) is

$$\frac{\text{Axial Load Above Cutout} - \text{Bending Load Above Cutout}}{\text{Axial Load Above Cutout}}$$

With the Loads Calculated Using N_x Values Along Row One Above the Cutout at Buckling.

Figure 33. Calculated Loading Ratio Above Cutout vs Change in Length For A Stiffened Cylinder

V. Conclusions

From the analysis undertaken in this study, the following conclusions can be made.

- (1) The Skogh-Brogan routine for applying pure bending rotations to a cylinder using end boundary kinematic constraints does keep the edge circular and planar under loading.
- (2) When the pure bending loads are applied to short unstiffened cylinders ($L/R < 10$) the structure assumes deformation patterns different from long cylinder bending deflections. The material on the tension zone (-90°) deforms inwards; whereas, the material on the compression zone ($+90^\circ$) bulges outwards. These radial displacements are of equal magnitude but opposite in sign. The effect diminishes circumferentially to zero at the 0 and 180° points. The longitudinal extent of this deformation pattern changes both by degree and direction with cylinder length.
- (3) The inplane V deflections at the middle columns (0° and 180°) follow a "beam type" deflection path reaching a maximum at the center mid plane of the cylinder.
- (4) As the cylinder length increases the effects diminish until an $L/R = 20$ where there is no discernible deformation for the mesh spacing used. The de-

flections at this length follow "beam type" flexure.

- (5) Discrete ring stiffening at the ends of the cylinder did not appreciably alter the overall characteristics of the deformations; at least for the chosen stringer dimensions and positioning from the loaded edge.
- (6) When stringers were added, the deformation pattern was altered. The cylinder/stringer combination is stiff enough at the boundary to follow beam flexure behavior. However, with shorter lengths $L/R < 10$ there isn't enough material between the edges to allow for this flexure. Therefore, the cylinder's radial displacements follow a reversal of direction near the center mid section. However, the inplane V deflections at the middle column continues to follow the typical flexure pattern.
- (7) When cutouts are added to the stiffened cylinder under bending loading at the maximum compression and tension zones, the deformation pattern initially follows that for no cutout stiffened cylinders. As the cutout is approached, the cylinder loses its rigidity and the deformations become almost linear.
- (8) For buckling analysis, the tension zone has very little effect on the critical stresses of the maximum compression zone fibers. Adding a cutout in the tension zone does not alter the failure values.

- (9) The buckling stress intensity values for stiffened cylinders without cutouts under axial vs bending loading lie within 13% of each other for the L/R range of .698 to 1.361. Axial analysis can be used therefore to predict moment load failures to at least this percentage accuracy.
- (10) Bending vs axial analysis for stiffened cylinders with cutouts is less precise. The trend shows a convergence of critical values to within 9% as the length increases to $L/R = 1.361$. For L/R values > 1 , a load ratio graph along with axial data can be used to model bending loads above the cutout.

Bibliography

1. Aksel'rad, E. L. "Refinement of the Upper Critical Loading of Pipe Bending Taking Account of the Geometric Nonlinearity." (In Russian), *Izvestia, Akademiia Nauk, SSSR, Otdelenie T Tekhnicheskikh Nauk, Mekhanika*, No. 4: 123-139, 1965.
2. Almroth, B. O. and Brogan, F. A. "Bifurcation Buckling as an Approximation of the Collapse Load for General Shells." *AIAA Journal*, Vol. 10, No. 4: 463-467, April 1972.
3. Almroth, B. O. and Brogan, F. A. "Numerical Analysis of Structures (Discretization Procedures)." Lockheed Missiles and Space Company, Inc. Technical Report No. LMSC-D556462, January 1977.
4. Almroth, B. O. and Brogan, F. A. "The Stags Computer Cods." NASA Contractor Report 2950, 1978.
5. Almroth, B. O., et al. User Instructions for STAGS C." Structural Analysis of General Shells Vol. II and Vol. III, December 1975.
6. Almroth, B. O. and Bushnell D. "Computer Analysis of Various Shells of Revolution." *AIAA Journal*, Vol. 6: 1846-1855, October 1968.
7. Almroth, B. O. and Starnes, J. H., Jr. "The Computer in Shell Stability Analysis." Journal of the Engineering Mechanics Division, 873-888, December 1975.
8. Anderson, J. K. and Peterson, J. P. "Buckling Tests of Two Integrally Stiffened Cylinders Subjects to Bending." NASA Technical Note D-6271, June 1971.
9. Batdorf, S. B. "A Simplified Method of Elastic-Stability Analysis for their Cylindrical Shells." NASA Technical Note No. 1342, 1947.
10. Block, D. L. "Buckling of Eccentrically Stiffened Orthotropic Cylinders Under Pure Bending." NASA Technical Note D-3351, March 1966.
11. Brazier, L. G. "On the Flexure of Thin Cylindrical Shells and other 'thin' sections." *Proceedings of the Royal Society, Series A*, 116: 104-114 (1926).

12. Brogan, F. A. and Almroth, B. O. "Buckling of Cylinders with Cutouts." AIAA Journal, Vol. 8: 236-240, February 1970.
13. Brush, D. O. "Prebuckling Rotations and Buckling Analysis." Proceedings of the ASCE Third Engineering Mechanics Division Specialty Conference, 77-80, September 1979.
14. Brush, D. O., and Almroth, B. O. Buckling of Bars, Plates and Shells. New York: McGraw-Hill, 1975.
15. Compton, N. L. "Nonlinear Collapse of Cylindrical Shells." Master's thesis, Air Force Institute of Technology, WPAFB, OH, 1977.
16. Donnell, L. H. "Stability of Thin-Walled Tubes under Torsion." NACA Technical Report No. 479: 95-116, 1933.
17. Gould, P. L. Static Analysis of Shells. Lexington Books, D. C. Heath and Company, 1977.
18. Koiter, W. T. "Elastic Stability and Post-buckling Behavior." Proc. Symp. Nonlinear Problems. University of Wisconsin Press, Madison, 257-275, 1963.
19. Lakshmikantham, C., Gerard, G. and Milligan, R. "General Instability of Orthotropically Stiffened Cylinders, Part II, Bending and Combined Compression and Bending." Air Force Flight Dynamics Laboratory Technical Report TR 65-161, August 1965.
20. Military Standardization Handbook, "Metallic Materials and Elements for Aerospace Vehicle Structures." MIL-HDRK-5C, Vols. I and II, 15 September 1979.
21. Nelson, D. A. "Buckling of Axially Compressed Stringer Stiffened Cylindrical Shells with and Without Cutouts." Master's Thesis, Air Force Institute of Technology, WPAFB, Ohio, December 1975.
22. Palazotto, A. N. "Bifurcation and Collapse Analysis of Stringer and Ring-Stringer Stiffened Cylindrical Shells with Cutouts." Computers and Structures, Vol. 7: 47-58.
23. Reedy, B. D. "An Experimental Study of the Plastic Buckling of Circular Cylinders in Pure Bending." International Journal of Solids Structures. Vol. 15: 669-683, 1979.

24. Reedy, B. D. and Calladine, C. R. "Classical Buckling of a Thin-Walled Tube Subjected to Bending Moment and Internal Pressure." International Journal of Mechanical Sciences, Vol. 20, No. 9: 641-650, 1978.
25. Saada, A. S. Elasticity: Theory and Applications. Pergamon Unified Engineering Series, Pergamon Press, Inc., 1974.
26. Seide, P. and Weingarten, V. I. "On the Buckling of Circular Cylindrical Shells Under Pure Bending." Journal of Applied Mechanics, Vol. 28: 112-116, 1961.
27. Singer, J. "Buckling of Integrally Stiffened Cylindrical Shells--A Review of Experiment and Theory." Presented at Van Der Neut Symposium, 1972.
28. Singer, J., et al. "On the Stability of Eccentrically Stiffened Cylindrical Shells under Axial Compression." International Journal of Solids Structures, 3: 445-470.
29. Skogh, J. and Brogan, F. "Collapse and Buckling of Finite Length Pipe Bends." Lockheed Palo Alto Research Laboratory, 20 December 1978.
30. Sobel, L. H. "On the Basic Concepts of the Instability of Structures." U.S. Atomic Energy Commission, E(11-1)-3045, September 1976.
31. Sobel, L. H. "On the Buckling of Cylindrical Shells Under Pure Bending." U.S. Atomic Energy Commission, E(11-1)-3045, November 1975.
32. Stephens, W. B. and Starnes, J. H. and Almroth, B. O. "Collapse of Long Cylindrical Shells under Combined Bending and Pressure Loads." AIAA Journal, 13: 20-25, January 1975.

AD-A079 853

AIR FORCE INST OF TECH WRIGHT-PATTERSON AFB OH SCH00--ETC F/6 20/11
A STUDY OF SHORT CYLINDRICAL SHELLS WITH AND WITHOUT CUTOUTS UN--ETC(U)
DEC 79 C J BANG
AFIT/GA/AA/797-1

UNCLASSIFIED

NL

2 of 2

ADA
679 863



END
PAGE
FILMED
2-80
DDI

Appendix A

Force and Moment Intensities, Constitutive Equations, and Kinematic Relations

The internal forces and moments for a shell are usually expressed in terms of forces and moments per unit distance along the edge of the shell element. These force and moment intensities, pictured on Fig 1, are related to the stresses as shown on the next page. The symbols $\underline{\sigma}_x$ and $\underline{I}_{x\theta}$ denote stress components at any point through the shell wall thickness.

The following page contains the kinematic middle-surface relations postulated by Donnell and the constitutive equations for thin-walled isotropic elastic cylinders. The form of these equations is taken from (14).

Force and Moment Intensities

$$N_x = \int_{-t/2}^{t/2} \underline{\sigma}_x \left(1 + \frac{z}{R}\right) dz$$

$$N_\theta = \int_{-t/2}^{t/2} \underline{\sigma}_\theta dz$$

$$N_{x\theta} = \int_{-t/2}^{t/2} \underline{\tau}_{x\theta} \left(1 + \frac{z}{R}\right) dz$$

$$N_{\theta x} = \int_{-t/2}^{t/2} \underline{\tau}_{\theta x} dz$$

$$Q_x = \int_{-t/2}^{t/2} \underline{\tau}_{xz} \left(1 + \frac{z}{R}\right) dz$$

$$Q_\theta = \int_{-t/2}^{t/2} \underline{\tau}_{\theta z} dz$$

$$M_x = R \int_{-t/2}^{t/2} \underline{\sigma}_x \left(1 + \frac{z}{R}\right) z dz$$

$$M_\theta = R \int_{-t/2}^{t/2} \underline{\sigma}_\theta z dz$$

$$M_{x\theta} = R \int_{-t/2}^{t/2} \underline{\tau}_{x\theta} \left(1 + \frac{z}{R}\right) z dz$$

$$M_{\theta x} = R \int_{-t/2}^{t/2} \underline{\tau}_{\theta x} z dz$$

Middle-Surface Kinematic Relations

$$\epsilon_x = u_{,x} + \frac{1}{2}\beta_x^2 \quad \beta_x = -w_{,x} \quad \kappa_x = \beta_{x,x}$$

$$\epsilon_\theta = \frac{v_{,\theta} + w}{R} + \frac{1}{2}\beta_\theta^2 \quad \beta_\theta = -\frac{w_{,\theta}}{R} \quad \kappa_\theta = \frac{\beta_{\theta,\theta}}{R}$$

$$\gamma_{x\theta} = \left(\frac{u_{,\theta}}{R} + v_{,x} \right) + \beta_x \beta_{\theta,y} \quad \kappa_{x\theta} = \frac{1}{2} \left(\frac{\beta_{x,\theta}}{R} + \beta_{\theta,x} \right)$$

Constitutive Equations

$$N_x = C(\epsilon_x + \nu \epsilon_\theta)$$

$$M_x = D(\kappa_x + \nu \kappa_\theta)$$

$$N_\theta = C(\epsilon_\theta + \nu \epsilon_x)$$

$$M_\theta = D(\kappa_\theta + \nu \kappa_x)$$

$$N_{x\theta} = C \frac{1 - \nu}{2} \gamma_{x\theta}$$

$$M_{x\theta} = D(1 - \nu) \kappa_{x\theta}$$

Appendix B

STAGSC PROGRAM LISTINGS

The following listings show the different aspects of the STAGSC computer code I used. They do not come from the same program.

B1 is a listing of the input data cards needed to run a program. This run was for a cylinder of total length 40 inches with a mesh arrangement of 16 by 71 over the quarter shell segment model. It has options included for bifurcation analysis of a dummy branch moment loaded cylinder with a wall subroutine defined surface with 12 inch cutouts.

B2 details the user written subroutine UCONST for a cylinder segment having 61 columns.

B3 shows the user written subroutine WALL with no cutouts.

B4 shows the user written subroutine WALL with two cutouts.

B5 details the subprogram MOMENT which calculates the total applied moment from the N_x values along the top row of the cylinder.

INPUT DATA CARDS

ALUM CYL - 15BY71 - 20BY180, 12 CUT, WSM STIFF, MOMENT 0.11, BIFURCATION

1, 2, 1, 0, 2, 208	B1
16, 71, 2, 2	C1
1, 0, 0, 0, 1, 0, 0	C2
1, 0, 2, 750, 0	E1
0, 0, 0, 0, 0, 2	F2
5, 1, 0, 0, 0, 0	F3
0, 0, 20, 0, -90, 0, 90, 0, 57.2958	I1
2, 3, 1	I2
5, 0, 15, 0	J1
5, 10	J2
15, 0, 15, 0, 15, 0	J3
10, 50, 10	J5
3, 4, 4, 4	J6
1, 0	K1
0, 0, -1, 2, 1, 36	L1
1, 0, 0, 0, 10.4E+6, 3.75E+6, .100, 0.0	-2
.28, .01493, .002858, 0.0, .008081, 0.0, -.45, 0.0	V1
0, 1, 1, 1, 0, 1	M3
1, 0	D1
2, 1, 0, 0, 1, 0	P1
0, 0, 1.0, 0.0, 1.0	I1
0, 0, 0	I2
1, 4, 4, 4	J1
1, 0	K1
.01, -1, 1, 1, 0	L1
0, 1, 0, 0, 0, 0	L2
3, 0	D1
1, 1, 0.0	P1
0.1, 10.4E+6	P2A
.33	P2B
0.0	
3.75E+6	
.03	
.1033	

B1

UCONST

SUBROUTINE UCONST

PURE MOMENT - EDGE STAYS CIRCULAR AND IN ONE PLANE

INPUT IS U DISPLACEMENT AT ROW1/COL1 ON DUMMY BRANCH 2

```

DIMENSION IBRNCH(5), IX(5), IY(5), ID(5), CC(5), T4A(51)
DATA T4A/-90., -87., -84., -81., -78., -75., -72., -69., -66.,
C  -63., -60., -57., -54., -51., -48., -45., -42., -39., -36.,
C  -33., -30., -27., -24., -21., -18., -15., -12., -9., -6., -3.,
C   0., 3., 6., 9., 12., 15., 18., 21., 24., 27., 30., 33.,
C  36., 39., 42., 45., 48., 51., 54., 57., 60., 63., 66., 69.,
C  72., 75., 78., 81., 84., 87., 90./
E = 10.*E+6
IX(1) = 1
IX(3) = 1
DO 10 I=1,61
TH = T4A(I)*3.14159256/180.
IX(2) = 1
IBRNCH(1) = 1
IBRNCH(2) = 1
IBRNCH(3) = 1

```

THIS SECTION PREVENTS SINGULARITIES

IF(I.E2.31) GO TO 5

IF(I.E2.1) GO TO 2

IF(I.E2.51) GO TO 2

EQUATION 1

```

IY(1) = I
ID(1) = 2
CC(1) = -SIN(TH) * E
IY(2) = I
ID(2) = 3
CC(2) = COS(TH) * E
CALL CONSTR (2,IBRNCH,IX,IY,ID,CC)
2 CONTINUE

```

B2

UCONST cont.

EQUATION 2

```
IY(1) = 31
ID(1) = 2
CC(1) = +E
IY(2) = I
ID(2) = 2
CC(2) = -COS(TH)*E
IY(3) = I
ID(3) = 3
CC(3) = -SIN(TH)*E
CALL CONSTR (3,IBRNCH,IX,IY,ID,CC)
```

EQUATION 3

```
IY(1) = 31
ID(1) = 1
CC(1) = E
IBRNCH(2) = 2
IX(2) = 1
IY(2) = 1
ID(2) = 1
CC(2) = SIN(TH)*E
IY(3) = I
ID(3) = 1
CC(3) = -E
CALL CONSTR (3,IBRNCH,IX,IY,ID,CC)
5 CONTINJE
10 CONTINUE
RETURN
END
```


WALL - NO CUTOUTS

```
SUBROUTINE WALL(IBRNCH,X,Y,Z,ICFB,ISTFF,IPRW,RHOA,C33)  
COMMON/LAYD1/ TL(20),EX3(20),EY3(20),U21(20),G3(20),ZET3(20),  
1RHO3(20),LAYS,LSTRS
```

```
COMMON/SHEAR/NSTI,ITYP(5),IDIR(5),SPACE(5),ANGE(5)
```

C

```
IF (IBRNCH.NE.1) RETURN
```

```
LAYS = 1
```

```
ICFB = 3
```

```
IPRW = 0
```

C

```
PANEL DATA
```

```
TL(1) = 0.1
```

```
EX3(1) = 10400000.
```

```
EY3(1) = 10400000.
```

```
U21(1) = .33
```

```
G3(1) = 3750000.
```

```
ZET3(1) = 0.0
```

```
RHO3(1) = 0.1
```

C

```
SMEARED DATA
```

```
ISTFF = 1
```

```
NSTI = 1
```

```
ITYP(1) = 1
```

```
IDIR(1) = 1
```

```
SPACE(1) = 3.0
```

```
RETURN
```

```
END
```

B3

WALL - TWO CUTOUTS

```

SUBROUTINE WALL( IBRNCH, X, Y, Z, ICFB, ISTFF, IPRW, RHOA, C)
COMMON /_AYD1/ TL(20), EX3(20), EY3(20), U21(20), G3(20), ZET3(20),
1 RHO3(20), LAYS, LSTRS
COMMON /SHEAR/ NSTI, ITYP(5), IDIR(5), SPACE(5), ANGE(5)
IF (IBRNCH.NE.1) RETURN
LAYS = 1
ICFB = 3
IPRW = 0
CUTOUT LOCATION TESTS FOR 12BY12 INCH CUT
BOTTOM LEFT
IF (X .GT. 14.00 .AND. Y .LT. -84.00) GO TO 10
BOTTOM RIGHT
IF (X .GT. 14.00 .AND. Y .GT. 84.00) GO TO 10
PANEL DATA
TL(1) = 0.1
EX3(1) = 10400000.
EY3(1) = 10400000.
U21(1) = .33
G3(1) = 3750000.
ZET3(1) = 0.0
RHO3(1) = 0.1
SHEARED DATA
ISTFF = 1
NSTI = 1
ITYP(1) = 1
IDIR(1) = 1
SPACE(1) = 3.0
GO TO 30
10 CONTINUE
CUTOUT DATA
ISTFF = 0
TL(1) = 0.1
EX3(1) = 0.0
EY3(1) = 0.0
U21(1) = 0.0
G3(1) = 0.0
ZET3(1) = 0.0
RHO3(1) = 0.0
30 CONTINUE
RETURN
END

```

B4

MOMENT

```

PROGRAM MOMENT(INPUT, OUTPUT, TAPE3=INPUT, TAPE4=OUTPUT)
2 READ (3,1) A
1 FORMAT (2EX,A2)
  IF (A.NE.2HXX) GO TO 2
  SMOMENT = 0.0
  DO 10 I = 1,91
    READ (3,3) A,X
    WRITE (4,3) A,X
3  FORMAT (8X,F8.4,4X,E12.6)
    AA = A*3.14159256/180.0
    IF ( I .EQ. 1 ) GO TO 20
    IF ( I .GT. 1 .AND. I .LT. 31 ) GO TO 30
    IF ( I .EQ. 31 ) GO TO 40
    IF ( I .EQ. 91 ) GO TO 50
    S = X * 1.5 * SIN(AA)
    GO TO 30
20 S = X * 1.5 * SIN(AA)
    GO TO 30
30 S = X * 3.0 * SIN(AA)
    GO TO 30
40 S = X * 2.25 * SIN(AA)
    GO TO 30
50 S = X * .75 * SIN(AA)
60 SMOMENT = SMOMENT + S
10 CONTINUE
  XX = 2.0 * 57.2958 * SMOMENT
  WRITE (4,4) XX
4  FORMAT (E12.6)
  STOP
END

```

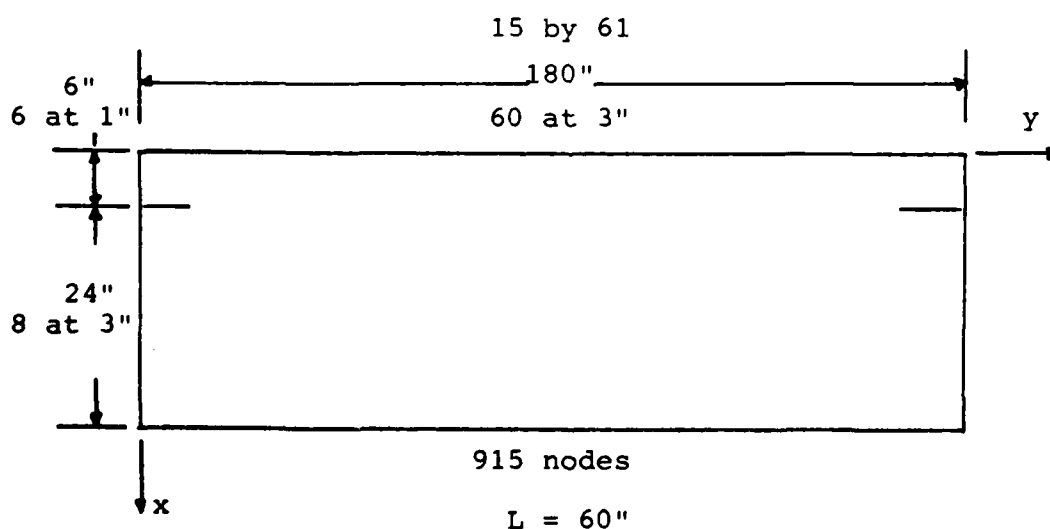
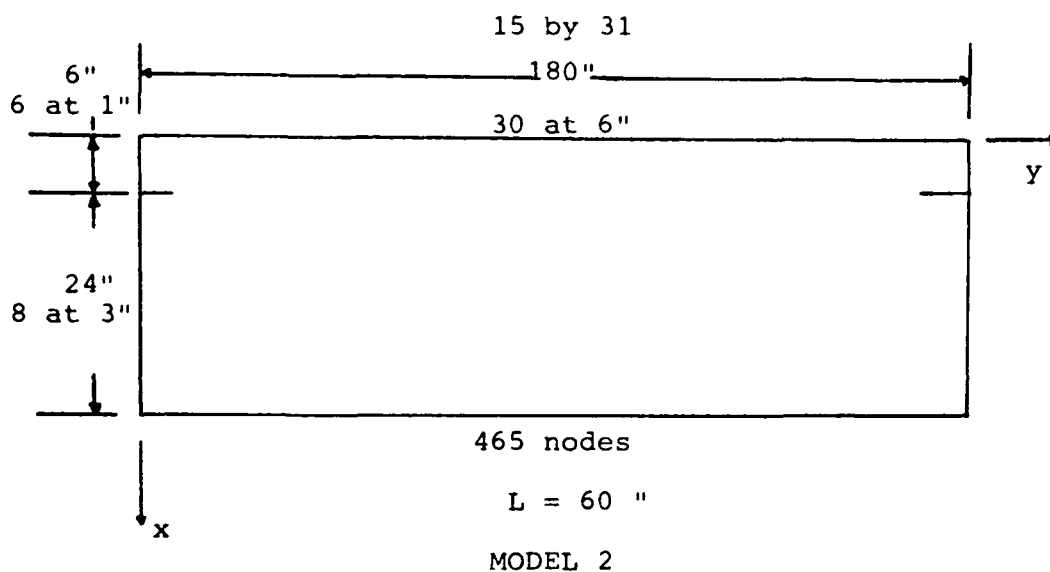
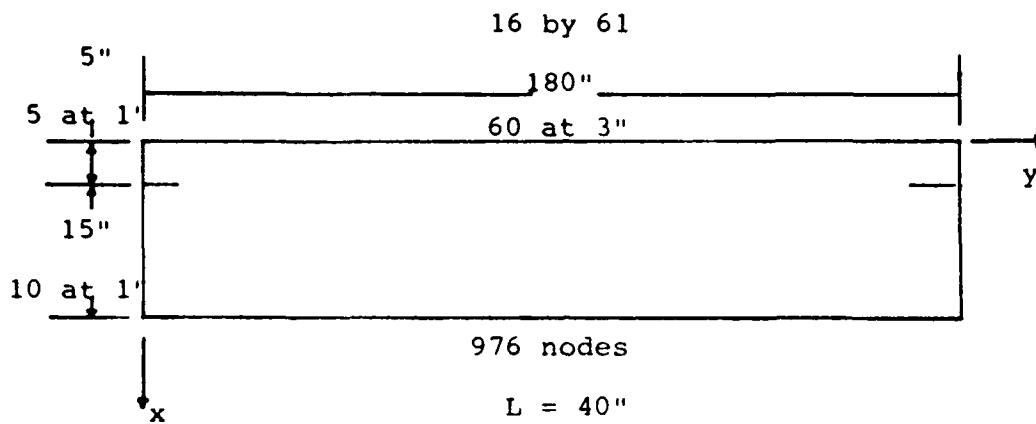
APPENDIX C

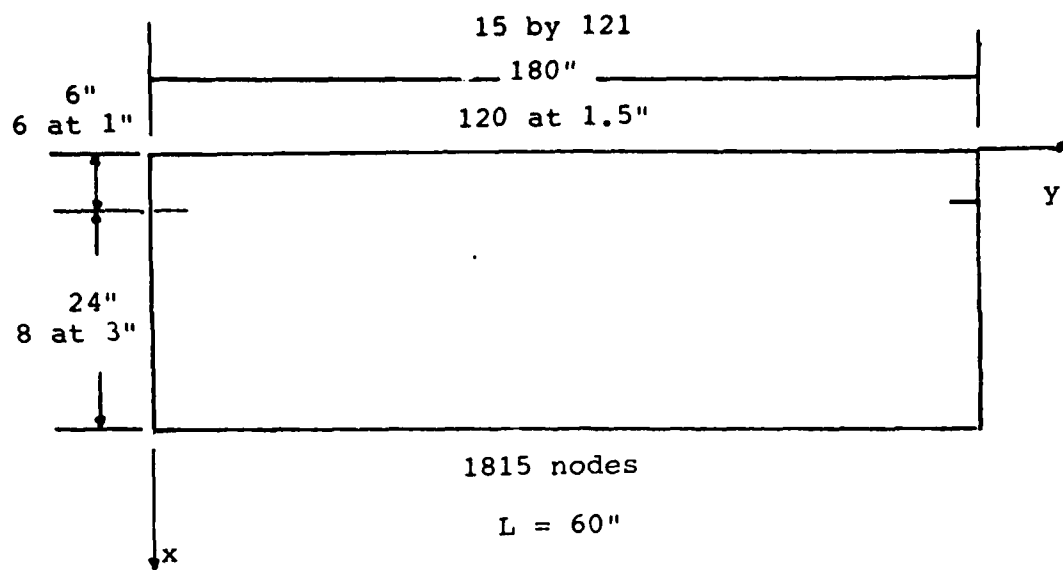
FINITE DIFFERENCE MESH ARRANGEMENTS

The different mesh arrangements are by model number. Models 1 to 15 and 2A pertain to unstiffened and stiffened shells without cutouts. Models 16 to 21A, B are used for the cutout analyses only.

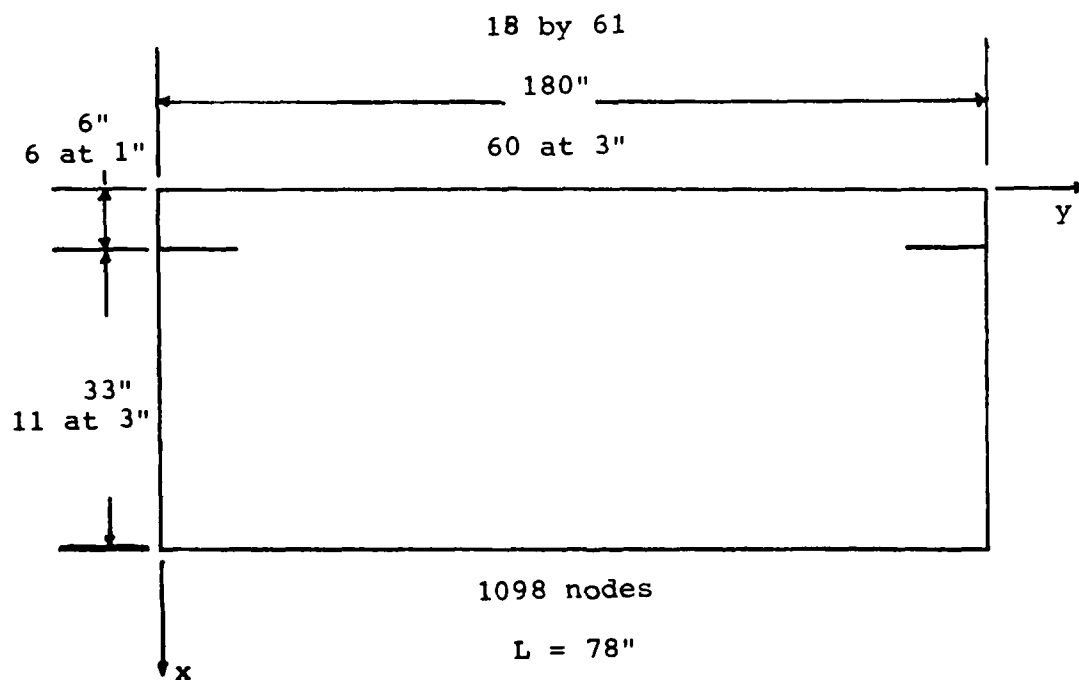
Model 3, the 15 by 61 mesh arrangement is the basic model around which the other non cutout models are compared. It gives a 3" by 3" square grid spacing for most of the cylinder segment with a 1" by 3" ratio for the top few rows. For the stiffened analyses, it gives results with a circumferential buckle wave pattern of 4 nodes per half sine wave, without having a grid line between each stiffener (economical). For unstiffened analysis it gives consistent although conservative buckling load results, approximately 78% of the classical value. Since the unstiffened analyses were mainly shape studies, these results are close enough. Models 8 to 15 were used for moment end deflection analysis only and not used for bifurcation studies.

Cutout models 16, 18, 20 are 1/8 shell Nelson models used for stiffened axial compression analysis. Models 17, 19 and 21 are used for the bending studies. The A and B suffixes refer to two cuts and one cut respectively. The dashed cutout is the one not there for one cut analysis.

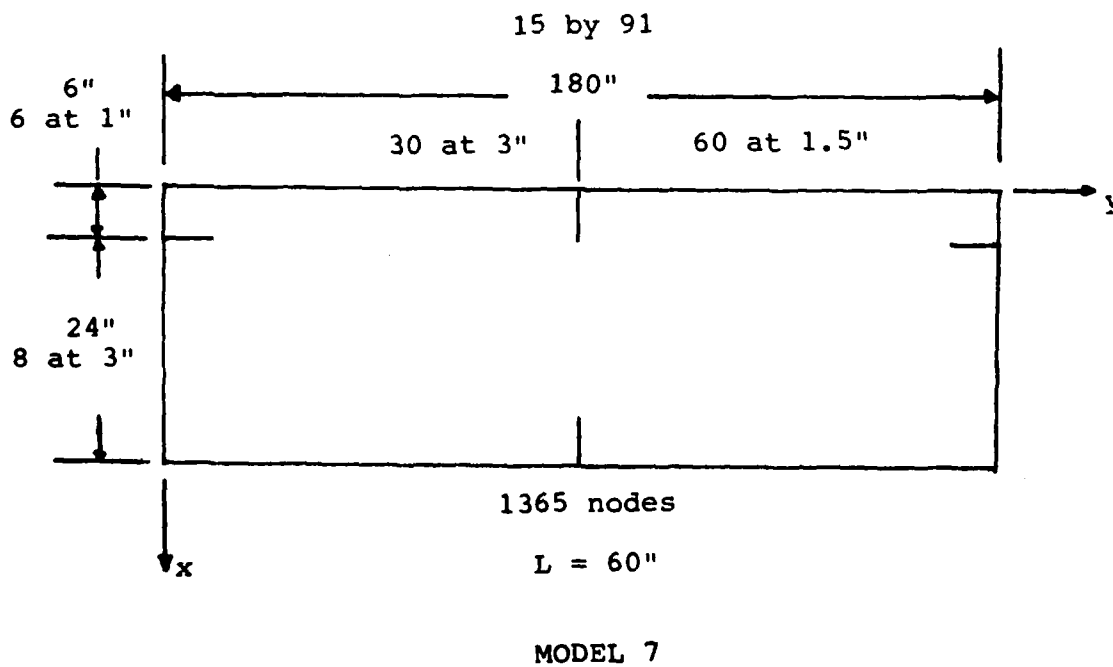
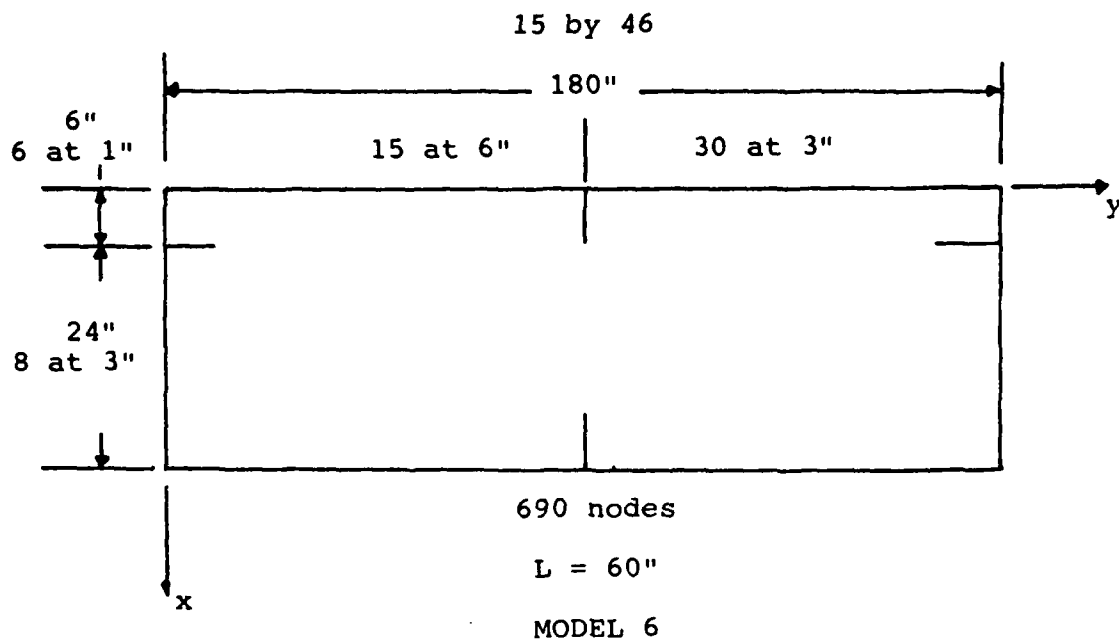




MODEL 4



MODEL 5



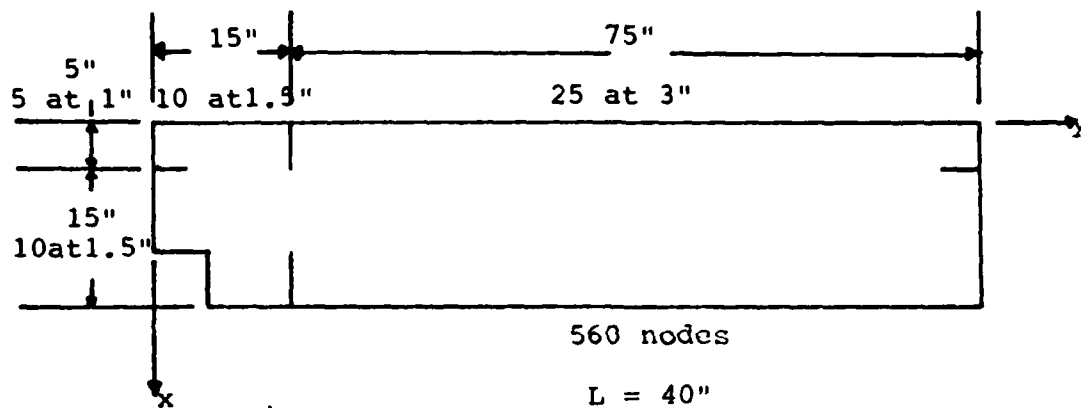
ADDITIONAL MODELS FOR SHELLS WITHOUT CUTOUTS

MODEL	SHELL WIDTH	Y DIRECTION MESH	NODES
2A	90"	30 at 3"	465

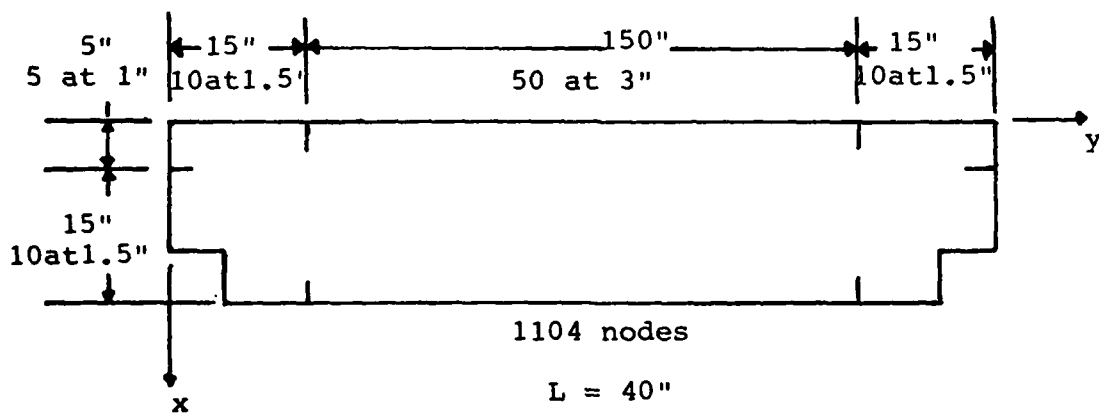
Note: x direction mesh remains the same for shell
length of 60"

MODEL	SHELL LENGTH	X DIRECTION MESH	NODES
8	120"	6 at 1" 9 at 6"	496
9	180"	5 at 1" 17 at 5"	713
10	240"	5 at 1" 23 at 5"	899
11	300"	6 at 1" 24 at 6"	961
12	360"	5 at 1" 25 at 7"	961
13	480"	6 at 1" 26 at 9"	1023
14	600"	3 at 1" 27 at 11"	961
15	1143"	3 at 1" 15 at 6" 48 at 12"	1829

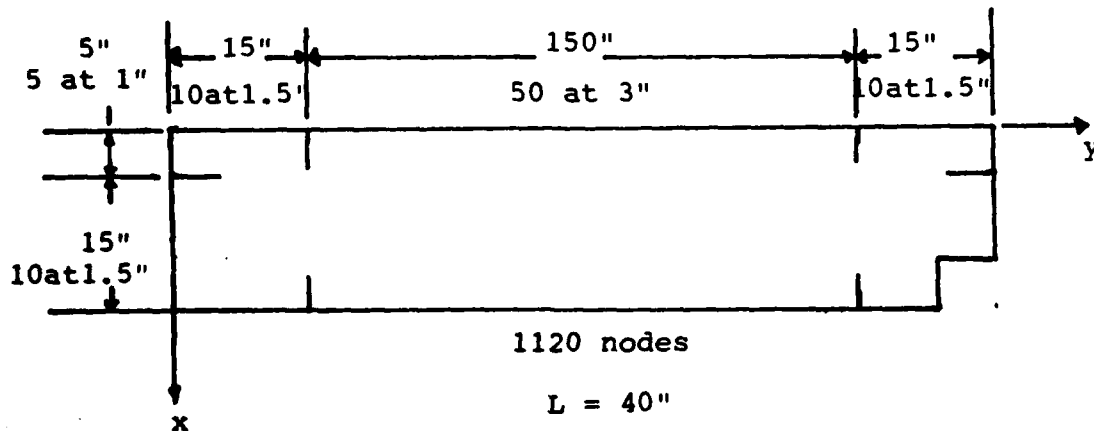
Note: Y direction mesh remains the same 30 at 6".



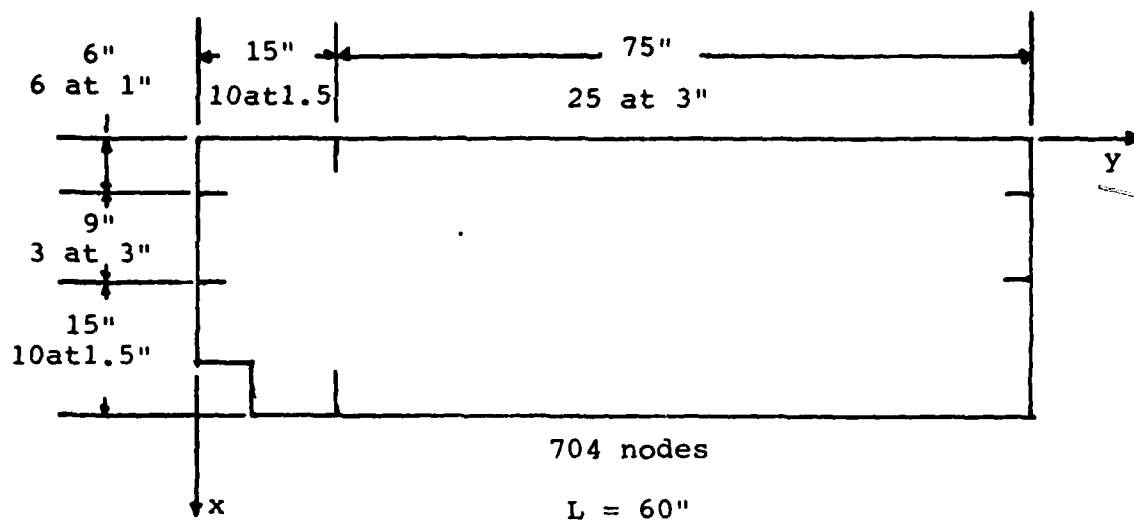
MODEL 16 16 by 36 (1 Cut)



MODEL 17A 16 by 71 (2 cut)

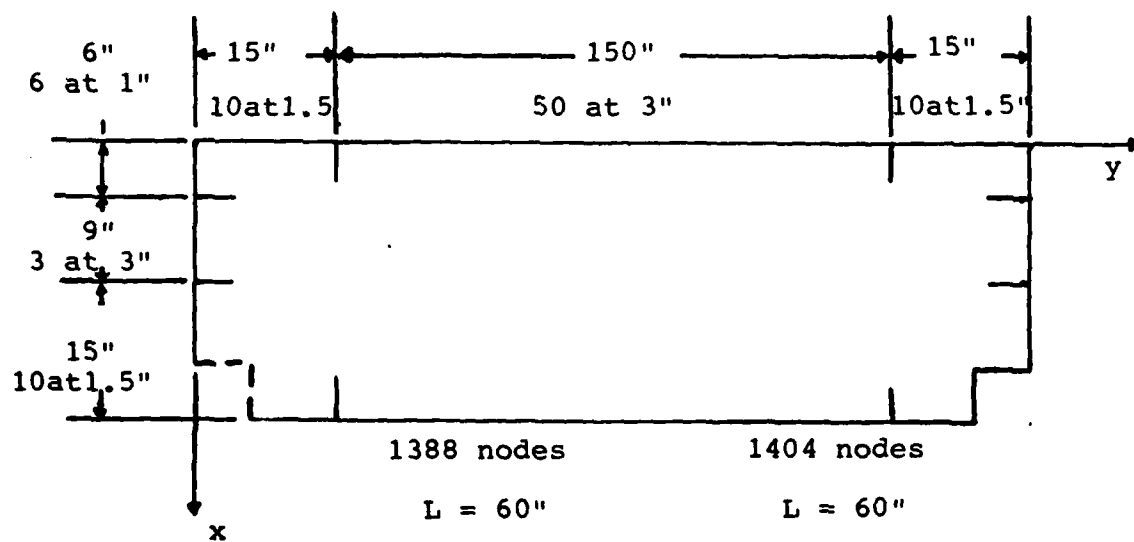


MODEL 17B 16 by 71 (1 Cut)



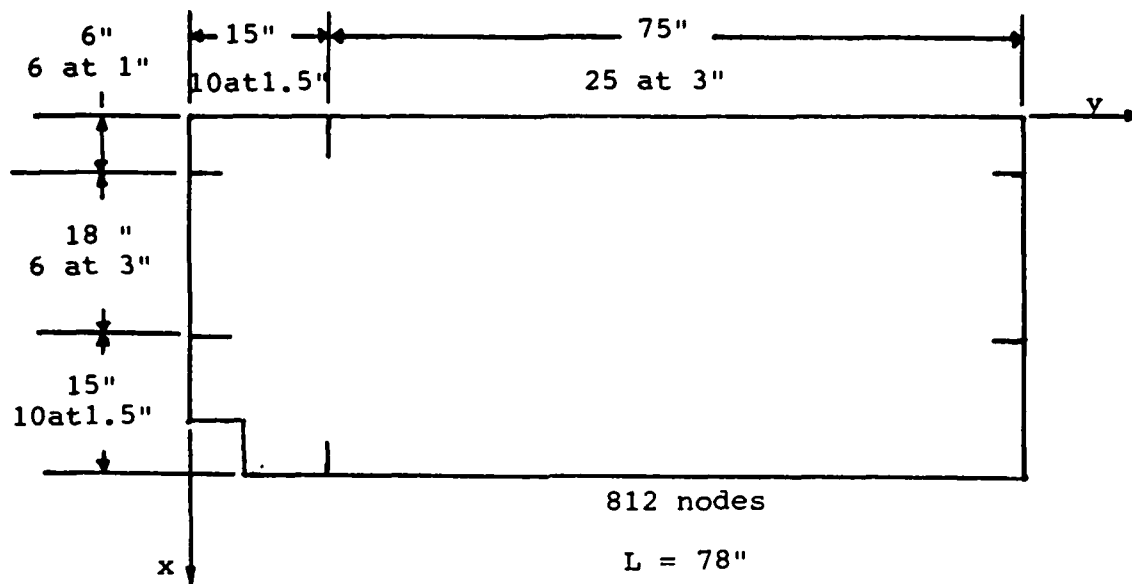
MODEL 18

20 by 36 (1 Cut)



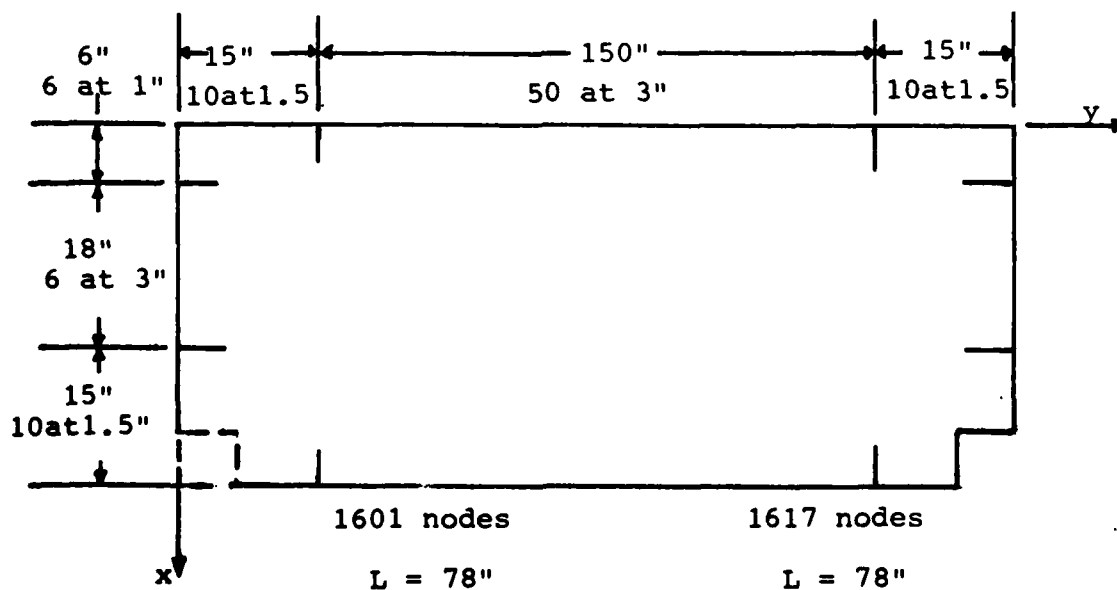
MODEL 19A (2 Cut)

MODEL 19B (1 Cut)



MODEL 20

23 by 36 (1 Cut)



MODEL 21A (2 Cut)

MODEL 21B (1 Cut)

Vita

Carl J. Bang was born on 8 May 1947 in Staten Island, New York City. He graduated from Tottenville High School in 1965 and attended one year of school at Cornell University. He then accepted a Congressional appointment to the Air Force Academy from which he received a Bachelor of Science Degree in Engineering Sciences in June 1970. After graduation, he completed pilot training at Vance AFB. He has served as a T-38 flight instructor and B-52 aircraft commander. He was a B-52 Wing Scheduler at Griffiss AFB prior to entering the School of Engineering, Air Force Institute of Technology, in June 1978.

PERMANENT ADDRESS: 810 N.E. 11th Avenue
Ocala, Florida 32670

UNCLASSIFIED

SECURITY CLASSIFICATION OF THIS PAGE (When Data Entered)

REPORT DOCUMENTATION PAGE		READ INSTRUCTIONS BEFORE COMPLETING FORM
1. REPORT NUMBER GA/aa/79D-1	2. GOVT ACCESSION NO.	3. RECIPIENT'S CATALOG NUMBER
4. TITLE (and Subtitle) A STUDY OF SHORT CYLINDRICAL SHELLS WITH AND WITHOUT CUTOUTS UNDER PURE BENDING		5. TYPE OF REPORT & PERIOD COVERED MS Thesis
		6. PERFORMING ORG. REPORT NUMBER
7. AUTHOR(s) Carl J. Bang Jr		8. CONTRACT OR GRANT NUMBER(s)
9. PERFORMING ORGANIZATION NAME AND ADDRESS Air Force Institute of Technology (AFIT/EN) Wright-Patterson AFB, Ohio 45433		10. PROGRAM ELEMENT, PROJECT, TASK AREA & WORK UNIT NUMBERS
11. CONTROLLING OFFICE NAME AND ADDRESS		12. REPORT DATE December 1979
		13. NUMBER OF PAGES 115
14. MONITORING AGENCY NAME & ADDRESS (if different from Controlling Office)		15. SECURITY CLASS. (of this report) Unclassified
		15a. DECLASSIFICATION/DOWNGRADING SCHEDULE
16. DISTRIBUTION STATEMENT (of this Report) Approved for public release; distribution unlimited		
17. DISTRIBUTION STATEMENT (of the abstract entered in Block 20, if different from Report)		
18. SUPPLEMENTARY NOTES Approved for public release; IAW AFR 190-17 Joseph P. Hipps, Major, USAF Director of Information		
19. KEY WORDS (Continue on reverse side if necessary and identify by block number) Pure Bending of Cylinders Cutouts Under Bending Stiffened Cylinders Buckling		
20. ABSTRACT (Continue on reverse side if necessary and identify by block number) In this report, short cylindrical shells are studied under pure bending. An edge kinematic constraint loading method is adapted for use with the STAGSC computer code. With it, short unstiffened cylindrical shells are studied for prebuckling displacements and compared with axially stressed cylinders. End rings are added to note their influence. The bending is applied to short internally stiffened (smeared stringer theory) cylinders with the resulting buckling values and patterns contrasted.		

DD FORM 1 JAN 73 1473

EDITION OF 1 NOV 65 IS OBSOLETE

UNCLASSIFIED

SECURITY CLASSIFICATION OF THIS PAGE (When Data Entered)

SECURITY CLASSIFICATION OF THIS PAGE(When Data Entered)

aga loading. The L/R range of interest is from .698 to symmetrical and unsymmetrical 12 inch cuts are added to a cylinder to study the resulting effects from this condition. The results indicate.

For short length ($L/R \leq 10$) cylinders, end loading by a point load causes structural deformation patterns different from long cylinder bending deflections.

The imposed boundary effect for unstiffened cylinders diminishes with L/R increase until $L/R = 20$ where there is no deformation influence.

Adding stiffeners studied did not alter the basic shear deformation patterns.

Local buckling failure under bending can be modified by axial compression analysis. ↵

UNCLASSIFIED

SECURITY CLASSIFICATION OF THIS PAGE(When Data Entered)